

Analysis of CO in the tropical troposphere using Aura satellite data and the GEOS-Chem model: insights into transport characteristics of the GEOS meteorological products

Junhua Liu¹, J. A. Logan¹, D. B. A. Jones², N. J. Livesey³, I. Megretskia¹, C. Carouge¹, and P. Nedelec⁴

¹School of Engineering and Applied Sciences, Harvard University, Cambridge, Massachusetts, USA

²Department of Physics, University of Toronto, Toronto, Ontario, Canada

³Jet Propulsion Laboratory, Pasadena, CA, USA

⁴CNRS-Laboratoire d'Aérologie, Toulouse, France

Received: 3 August 2010 – Published in Atmos. Chem. Phys. Discuss.: 20 August 2010

Revised: 24 November 2010 – Accepted: 13 December 2010 – Published: 23 December 2010

Abstract. We use the GEOS-Chem chemistry-transport model (CTM) to interpret the spatial and temporal variations of tropical tropospheric CO observed by the Microwave Limb Sounder (MLS) and the Tropospheric Emission Spectrometer (TES). In so doing, we diagnose and evaluate transport in the GEOS-4 and GEOS-5 assimilated meteorological fields that drive the model, with a particular focus on vertical mixing at the end of the dry season when convection moves over the source regions. The results indicate that over South America, deep convection in both GEOS-4 and GEOS-5 decays at too low an altitude early in the wet season, and the source of CO from isoprene in the model (MEGAN v2.1) is too large, causing a lag in the model's seasonal maximum of CO compared to MLS CO in the upper troposphere (UT). TES and MLS data reveal problems with excessive transport of CO to the eastern equatorial Pacific and lofting in the ITCZ in August and September, particularly in GEOS-4. Over southern Africa, GEOS-4 and GEOS-5 simulations match the phase of the observed CO variation from the lower troposphere (LT) to the UT fairly well, although the magnitude of the seasonal maximum is underestimated considerably due to low emissions in the model. A sensitivity run with increased emissions leads to improved agreement with observed CO in the LT and middle troposphere (MT), but the amplitude of the seasonal variation is too high in the UT in GEOS-4. Difficulty in matching CO in the LT and UT implies there may be overly vigorous vertical mixing in GEOS-4 early in the wet season. Both simulations and observations show a time lag between the peak in fire emissions (July and August) and in CO (September and October). We argue that

it is caused by the prevailing subsidence in the LT until convection moves south in September, as well as the low sensitivity of TES data in the LT over the African Plateau. The MLS data suggest that too much CO has been transported from fires in northern Africa to the UT in the model during the burning season, as does MOZAIC aircraft data, perhaps as a result of the combined influence of too strong Harmattan winds in the LT and too strong vertical mixing over the Gulf of Guinea in the model.

1 Introduction

Atmospheric carbon monoxide (CO) is produced from incomplete combustion of fossil fuel and biofuels, biomass burning, and from oxidation of atmospheric methane and other hydrocarbons. It plays a critical role in controlling the oxidative capacity of the atmosphere through reaction with the primary tropospheric oxidant, the OH radical, and its oxidation provides a source or sink for ozone, depending on levels of nitrogen oxides (e.g., Levy, 1971; Crutzen, 1973; Logan et al., 1981). It also has an indirect radiative effect (Daniel and Solomon, 1998; Solomon et al., 2007). Carbon monoxide has a lifetime on the order of weeks in the tropics, considerably shorter than the inter-hemispheric mixing time of about a year. It has been used as a tracer to diagnose transport pathways of pollution in the tropical troposphere (e.g., Staudt et al., 2001; Edwards et al., 2006). The life time of CO in the tropical troposphere is longer than the time-scale for vertical transport by deep convection, so CO can also be used as a tracer of vertical transport. In this study, we use the GEOS-Chem chemistry-transport model (CTM) to interpret satellite observations of the spatial and temporal variations



Correspondence to: Junhua Liu
(jliu@seas.harvard.edu)

of CO in the tropical upper troposphere (UT) from 2005 to 2006. In so doing, we diagnose and evaluate transport in the model in the biomass burning season, with a particular focus on vertical mixing at the end of the dry season when convection moves over the source region.

Earlier work by Edwards et al. (2006) used MOPITT data and the MOZART model to examine transport of CO in the southern hemisphere in September–November. They discussed export of CO from biomass burning regions in the lower troposphere (LT), and showed the role of convection in the ITCZ in transporting CO to the UT using MOPITT data at 250 and 700 hPa, with a focus on the Indian Ocean.

Our study uses upper tropospheric CO measurements from the Microwave Limb Sounder (MLS) instrument on the Aura satellite, launched in July 2004 (Waters et al., 2006). The vertical resolution of the MLS data (~ 4 km) is higher than that of thermal infrared nadir sounding instruments such as MOPITT, and data are provided at 215, 147, and 100 hPa (Livesey et al., 2008). The MLS CO measurements have been used as a tracer of convection and large scale ascent in the UT and lower stratosphere (LS). Schoeberl et al. (2006) identified a tape recorder in MLS CO data in the stratosphere, and suggested that the semi-annual cycle of CO in the UT was determined by the seasonal variation of tropical biomass burning and convective detrainment; a model study confirmed this finding (Duncan et al., 2007). Liu et al. (2007) explored the spatial/temporal relationships among MLS CO, H₂O and deep convection, and argued that the CO maxima in March to May and September to November were caused by co-location of deep convection and biomass burning emissions over Africa and Amazonia. Jiang et al. (2007) examined the influence of deep convection and surface emissions on CO in the UT over Asia and the northern Pacific using MLS CO and ice-water content (IWC) measurements. There have also been several studies focused on transport to the UT over Asia during the monsoon season using MLS CO data (Li et al., 2005; Fu et al., 2006; Park et al., 2007, 2008, 2009), following the identification of a pronounced CO maximum at 147 hPa in late summer over India and Tibet (Filipiak et al., 2005).

Barret et al. (2008) assimilated MLS data in the MOCAGE Chemistry Transport Model (CTM) to investigate the transport pathways affecting CO in the UT over Africa in July 2006. They found that the CO maximum at ~ 200 hPa around 10° N is driven by deep convective uplift of air masses affected by biomass burning in southern Africa. However, above ~ 150 hPa, they argue that the broad CO maximum over northern Africa is strongly influenced by the large circulation associated with the Asian summer monsoon; pollution from S. E. Asia and India that is trapped in the Asian monsoon anticyclone is transported westward in the tropical easterly jet over northern Africa. These dynamical arguments are consistent with the findings of an analysis over the Mediterranean by Lelieveld et al. (2002).

The MLS data show maxima at 215 hPa over regions with biomass burning that are associated with convective activity (Liu et al., 2007). This is about the level with maximum outflow from convection, according to evidence from ozone profiles that show a minimum near 200 hPa (Folkens et al., 1999, 2002), and according to a recent review of transport in the tropical tropopause layer (TTL) by Fueglistaler et al. (2009). Above about 150 hPa, convective outflow decays rapidly with increasing height, and vertical motions are influenced by net radiative heating and the large scale flow, but considerable uncertainty remains in the profile of convective detrainment (Fueglistaler et al., 2009).

In this study we focus on vertical transport over the tropical continents, and exploit the spatial and temporal patterns evident in MLS CO in the UT that are clearly related to upward transport of biomass burning emissions. The MLS data, in combination with CO data for the LT, provide a valuable test of transport in global models. We demonstrate this using a state of the art global chemical transport model, GEOS-Chem, which is driven by assimilated meteorological fields from the Goddard Earth Observing System (GEOS) developed by the Global Modeling and Assimilation Office at NASA/Goddard (<http://gmao.gsfc.nasa.gov/>). We use the latest version of the GEOS fields, GEOS-5, and compare to results using GEOS-4 fields. The GEOS-4 fields have been used in many recent studies with GEOS-Chem, including those focused on the tropics (e.g., Martin et al., 2007; Sauvage et al., 2007b; Nassar et al., 2009).

In the GEOS data assimilation system, as other current general circulation models, deep convection is a sub-grid process that needs to be parameterized. Transport of tracers by convection and by advection are treated as separate operators in GEOS-Chem and other CTMs, even though they are inherently related (Lawrence and Salzmann, 2008). GEOS-4 uses the parameterization scheme of Zhang and McFarlane (1995) for deep convection and the Hack (1994) parameterization for shallow convection, while GEOS-5 uses the relaxed Arakawa-Schubert (RAS) scheme (Moorthi and Suarez, 1992). Folkens et al. (2006) explored the use of data for CO, O₃, and HNO₃ to test the convective parameterizations in an earlier version of the GEOS-Chem model, driven by GEOS-3 and GEOS-4 fields. Convection in GEOS-3 was also based on the RAS scheme, but with a different implementation from GEOS-5. Folkens et al. (2006) compared the model averages for 20° N–20° S to the mean of sparse aircraft data and ACE-FTS satellite data, and to mean sonde profiles for O₃. Their comparisons to ozone implied relatively weaker deep convective outflow in the RAS scheme in GEOS-3 than in the ZM scheme in GEOS-4. The data available at the time of their study was not sufficient to provide a thorough evaluation of the convective schemes.

In the LT, we use CO retrievals from the Tropospheric Emission Spectrometer (TES) to evaluate the GEOS-Chem simulations (e.g., Rinsland et al., 2006). The TES instrument is also on the Aura satellite. We evaluate model performance

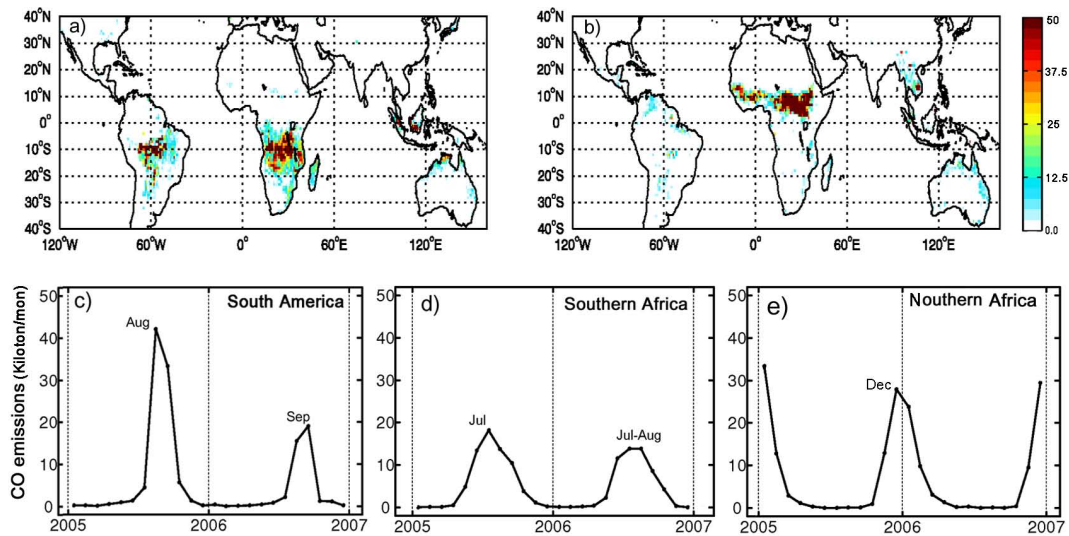


Fig. 1. Mean GFED v2 CO emissions ($\text{kiloton month}^{-1}$) averaged for (a) July–October of 2005–2006; (b) November 2005 to February 2006. Time evolution of regional CO emissions ($\text{kiloton month}^{-1}$) averaged over (c) South America; (d) southern Africa and (e) northern Africa.

by examining horizontal and vertical transport in the model. Our results provide in-depth understanding of how dynamics influences the CO re-distribution in the troposphere, and diagnose limitations of transport in the GEOS meteorological fields.

Sections 2 and 3 describe the model and satellite data. In Sect. 4, we show the spatial distribution and seasonal variation of CO observations and model simulations in the tropics in the LT and UT. In Sect. 5 we examine the influence of transport on CO in the UT, and show the sensitivity of model CO to the different convection schemes. We also identify the causes of discrepancies between model and observations, including deficiencies in transport and in sources of CO.

2 Model description

We use the GEOS-Chem version 8-02-04 global 3-D model with $4^\circ \times 5^\circ$ horizontal resolution, driven by the GEOS assimilated meteorological observations, versions GEOS-4 (Bloom et al., 2005) and GEOS-5 (Rienecker et al., 2007). The native resolution of the GEOS-4 fields is $1^\circ \times 1.25^\circ$ with 55 vertical levels, and that of the GEOS-5 fields is $0.5^\circ \times 0.667^\circ$ with 72 vertical levels; we regrid to $4^\circ \times 5^\circ$ for input to GEOS-Chem. A major difference between these two meteorological fields is their convective parameterization schemes, as noted above.

The emissions of CO in the GEOS-Chem model include anthropogenic, biofuel, biomass burning, and biogenic emissions. The sources of anthropogenic emissions are summarized in the recent study of Nassar et al. (2009). Biofuel emissions are from the inventory of Yevich and Logan (2003).

Biomass burning emissions are from the Global Fire Emission Database (GFED) version 2 (van der Werf et al., 2006). Emissions of CO and other tracers are derived by combining information on burned area for selected regions with fire hot spot data (Giglio et al., 2006), fuel burned from a biogeochemical model, and emission factors for each species. We used the 8-day emissions which were derived by resampling the inventory to an eight-day mean using MODIS fire counts (Giglio et al., 2003; <http://www.ess.uci.edu/~jranders/>). Figure 1 shows the GFED v2 CO emissions, for the main northern and southern dry seasons averaged over the years 2005–2006. Africa is typically the single largest continental source of biomass burning emissions. The northern biomass burning season occurs primarily from November to February, from the southern Sahel to about 4° S. The southern biomass burning season occurs primarily between June and October, moving slowly from central and western Africa (south of the equator) towards the south and east of the continent (Marengo et al., 1990; Giglio et al., 2006; Ito and Akimoto, 2007). South America is the other major burning region in the southern hemisphere. Figure 1c–e shows the temporal variations of CO emissions averaged over these three regions. The major fires start two months later in South America than that in southern Africa. In South America there was a drought in southwest Amazonia in 2005 caused in part by anomalously warm sea surface temperatures in the north tropical Atlantic (Marengo et al., 2008; Zeng et al., 2008), and CO emissions from fires that year were almost twice those in 2006. In southern Africa and northern Africa, the emissions have a smaller interannual variation.

We use the latest Model of Emissions of Gases and Aerosols from Nature (MEGAN) (Guenther et al., 2006) (version 2.1) to simulate isoprene emissions for each model

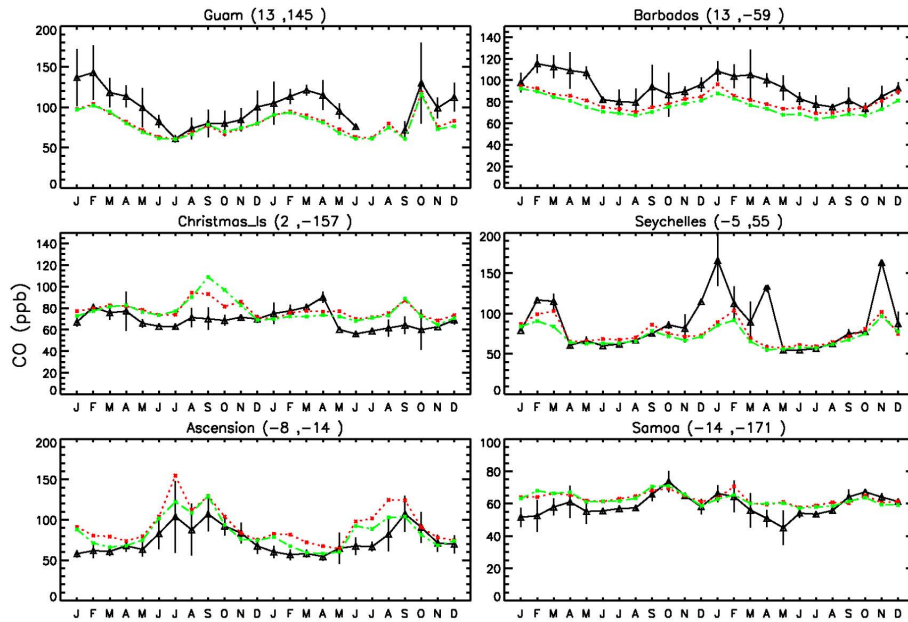


Fig. 2. Monthly variation of CO (ppb) from January 2005 to December 2006 at six tropical surface sites. Observations from the NOAA/GMD are in black (Novelli et al., 2003), GEOS-Chem model simulations are shown in red (GEOS-5) and in green (GEOS-4).

grid (Guenther and Wiedinmyer, 2007; Sakulyanontvittaya et al., 2008). This is a more recent version than that in the GEOS-Chem model described by Barkley et al. (2008), version 2 (v2006). MEGAN computes emissions for plant functional types (PFTs) as a function of temperature, solar radiation, leaf area index (LAI), and leaf age. Fractional cover for each PFT and vegetation-specific emission factors (EFs) are based on the MEGAN landcover data (PFT v2.0, EFs v2.0). The hybrid algorithm, which combines several parameterizations as described in Guenther et al. (2006) and Guenther and Wiedinmyer (2007) and Guenther et al. (1995, 1999) is applied in our standard model runs. This approach computes variations of light and leaf area at 5 sub-layers within a canopy through a canopy model. We also adopted a simplified parameterized canopy environment emission activity (PCEEA) algorithm, described in detail in Guenther et al. (2006) and Guenther and Wiedinmyer (2007), in a sensitivity run. Monthly mean LAI values are derived from Moderate Resolution Imaging Spectrometer (MODIS) Collection 5 (Shabanov et al., 2005). We drive MEGAN with assimilated surface air temperature and photosynthetically active radiation (direct and diffuse from the GEOS fields, and with MODIS LAI).

The lightning parameterization in the model is described by Murray et al. (2010). We use an updated profile for the lightning NO_x source following the vertical distribution functions based on a cloud resolving model transporting gases with resolved small scale motions, as described by Ott et al. (2009). Approximately 6.3 Tg N a⁻¹ NO_x are released globally.

In this study, we carried out simulations for January 2005 to December 2006 with O₃-NO_x-hydrocarbon chemistry driven by GEOS-4 and GEOS-5. The model runs were initialized in January 2004. We also conducted CO-only simulations with tagged sources and monthly mean of OH concentrations archived from the respective chemistry simulations. The methyl chloroform lifetime with respect to removal by tropospheric OH is 5.9 years in our model driven by GEOS-5, and 5.5 years in our model driven by GEOS-4, which are consistent with lifetimes derived from analysis of data for methyl chloroform (e.g., Prinn et al., 2001, 2005). In our tagged CO simulations, we use NO_x concentration fields saved from the respective chemistry simulations to calculate the yield of CO from isoprene (Miyoshi et al., 1994; Duncan et al., 2007). Initial conditions were taken from a 1-year spin-up starting in January 2004. Model time steps were set to 30 min for transport and convection and 60 min for emissions and chemistry.

Figure 2 compares the CO simulations driven by GEOS-5 (red), GEOS-4 (green) with observed monthly mean CO (black) from six tropical sites of the NOAA Earth System Research Laboratory, Global Monitoring Division (GMD) (Novelli et al., 2003). The simulations capture the observed phase of the seasonal cycles, but are too low in winter-spring in the northern hemisphere sites (Guam and Barbados), as found by previous studies using GEOS-Chem (Duncan et al., 2007; Kopacz et al., 2010) and other models (e.g. Shindell et al., 2006). At Christmas Island, the simulations display a maximum in September that is not present in the observations, while at Seychelles, in the Indian Ocean, the models

underestimate the maxima in late 2005/early 2006, and in November 2006. At Ascension Island, the model simulations match the phase of the observed CO, but are too high in austral winter.

3 Satellite data

Both TES and MLS are on the NASA EOS Aura satellite mission launched on 15 July 2004, in a near polar, sun-synchronous, 705 km altitude orbit with equator crossing at 1:45 pm local solar time and a 16-day repeat cycle. TES is an infrared Fourier transform spectrometer with high spectral resolution (0.1 cm^{-1}) and a wide spectral range ($650\text{--}3050 \text{ cm}^{-1}$) (Beer et al., 2001; Beer, 2006). A global survey (GS) of TES is obtained every other day and consists of 16 orbits ($\sim 26 \text{ h}$) of nadir observations spaced 1.6° apart with a footprint of $5.3 \times 8.3 \text{ km}^2$. Each orbit track in a GS is offset by 22° . Near global coverage is obtained after approximately 16 days with 8 GS.

TES retrievals are based on the optimal estimation approach (Rodgers, 2000) and are described in Worden et al. (2006) and Bowman et al. (2006), with error characterization described in Kulawik et al. (2006). We use Level 2, V003 TES data (F04_04). The retrieved profiles are provided on a 67-level vertical grid from the surface to 0.1 hPa. The number of statistically independent elements of the retrieval for CO, represented by the degree of freedom (DOF) (Rodgers, 2000), has varied over time, as a result of the variation of TES instrument alignment. From 29 November 2005 to 2 December 2006, the TES optical bench was warmed up to improve the TES beam splitter alignment. The procedure improved the measured signals, the total retrieval errors, and the retrieval precision for TES CO. The average DOFs between 30° N – 30° S was 0.72 prior to the TES optical bench warm up and then increased to 1.45 after the warm up (Rinsland et al., 2006). The TES CO data were screened using the recommended data quality flags given in the TES Level 2 Data User's guide, version 4.0 (Osterman, 2007), and we also removed profiles for which the effective cloud optical depth was greater than 3, or the cloud top pressure was less than 750 hPa (Worden et al., 2007).

The TES retrieval of CO (V002) was validated through comparisons with aircraft observations, showing agreement within 10%, within the TES retrieval errors (Luo et al., 2007a; Lopez et al., 2008). TES V002 and V003 are very similar to each other for the tropics and mid-latitudes (Osterman, 2007). The global patterns of TES CO are consistent with those measured by Measurement of Pollution in the Troposphere (MOPPIT) on the NASA Terra satellite (Luo et al., 2007b). The CO profiles retrieved from TES and MOPPIT agree within a few percent when compared appropriately, allowing for different a priori constraints and smoothing errors (Luo et al., 2007b; Ho et al., 2009).

The MLS instrument is a small radio telescope installed on the front of the Aura Satellite. It continuously measures thermal emission from broad spectral bands (118–2250 GHz) by 7 microwave receivers using a limb viewing geometry (Waters et al., 2006). MLS is radiometrically calibrated after every 25-s limb scan. It performs one scan every 1.5° along the Aura orbit. The MLS data used in this study are V2.2 Level 2, and we screen the data as recommended by Livesey et al. (2007). The data are provided on a fixed pressure grid with 6 levels per decade, with valid CO data at 215, 147, and 100 hPa in the UT.

Validation of V2.2 CO retrievals with aircraft data shows that the MLS CO is biased high by a factor of ~ 2 at 215 hPa, but that the morphology is generally realistic (Livesey et al., 2008). Much more limited aircraft data implies that MLS is biased high by about 30% at 147 hPa (Livesey et al., 2008).

To compare GEOS-Chem with TES retrieved profiles, we sampled the model profiles along the TES orbit track at the observation time, and interpolated them to the 67 pressure levels as logarithms of mixing ratios using the method described by Zhang et al. (2006). Since GEOS-Chem has poor predictive capability in the stratosphere, we replaced the simulated profiles above the model tropopause with the TES retrievals. To remove any artificial influence of the geographically variable a priori used in the retrieval, we reprocess the TES profiles using a universal a priori, produced by averaging the original TES a priori constraint for July 2006 in the tropical band (30° N to 30° S), as in Nassar et al. (2008). The procedure and its implications of using the uniform a priori are discussed in Kulawik et al. (2008). We smooth the model profiles using the TES averaging kernel (AK) and a priori profile to match the TES vertical resolution.

To compare GEOS-Chem with MLS retrieved profiles, we sampled the model profiles along the MLS orbit track at the observation time, interpolated the model profiles to the high resolution pressure grid (577 levels) and applied the MLS averaging kernel matrix to interpolate them to the MLS's 37 pressure levels (Livesey et al., 2007).

4 Spatial distribution of CO

4.1 Lower troposphere

Figure 3 shows the spatial pattern of CO at 681 hPa for the TES data and the GEOS-4 and GEOS-5 model results from August 2005 to March 2006, with similar results from August to December 2006 in Fig. 4. Over South America, TES CO is highest in September and October of 2005 and in September of 2006, with similar results in the GEOS-4 simulation in both years, and in the GEOS-5 simulation in 2006. The CO maximum lags the peak in CO emissions (Fig. 1) by one month. The models underestimate CO over Brazil, particularly in the months with highest CO, and overestimate CO over the Andes, south of 10° S . Over southern Africa,

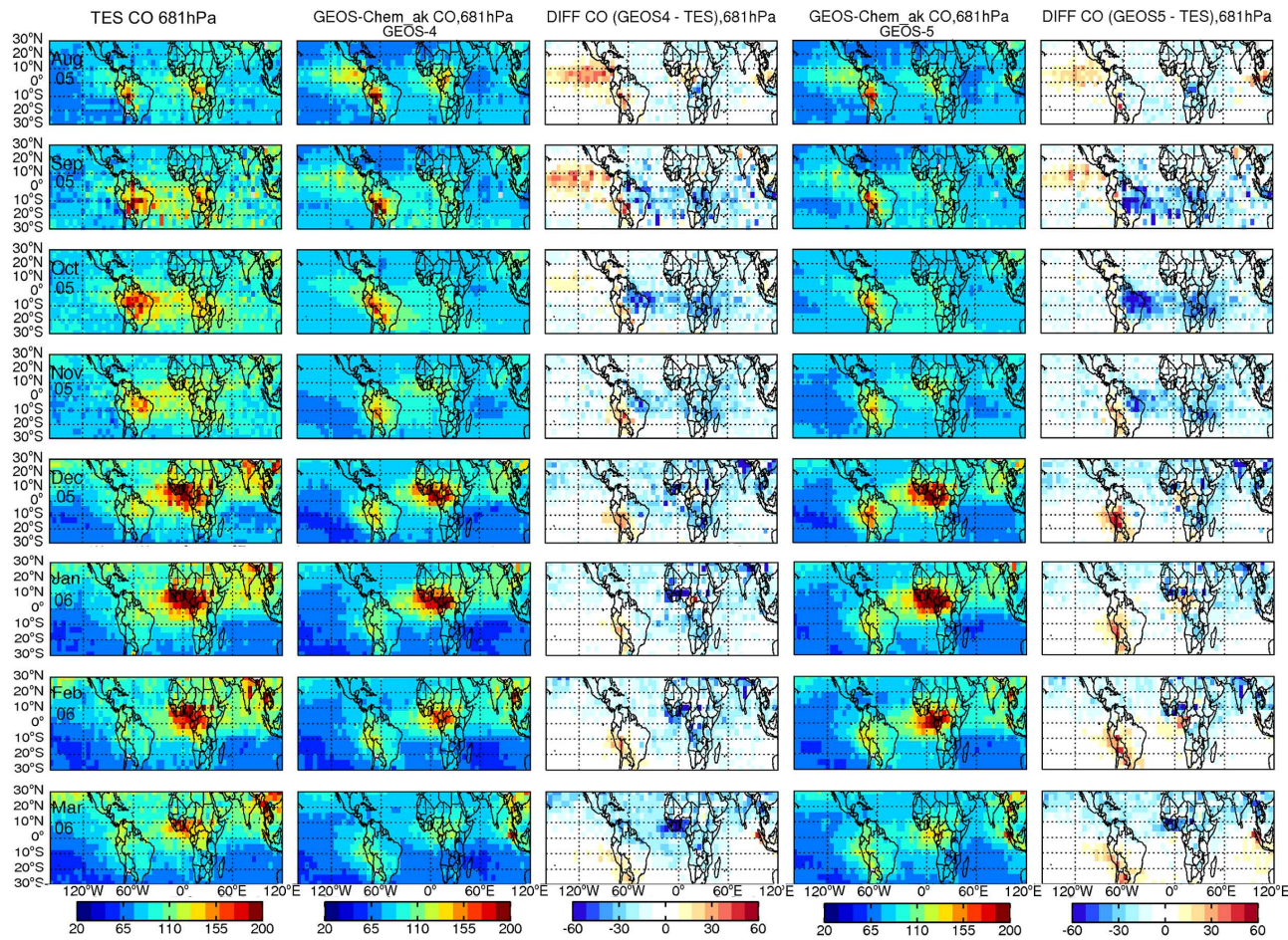


Fig. 3. Lower tropospheric CO at 681 hPa from August 2005 to March 2006 from TES (left column), the model driven by GEOS-4 with the TES averaging kernel (AK) applied, and the model wAK-TES difference (2nd and 3rd columns), the model driven by GEOS-5 with the TES AK, and the model wAK-TES difference (the 4th and 5th columns).

there is a broad maximum from August to October in the TES data and the models, and there is a large underestimate in model CO. Kopacz et al. (2010) found similar underestimates in biomass burning regions in GEOS-Chem simulations for May 2004 to April 2005, using GEOS-4. The results of their multi-satellite inversion (AIRS, MOPITT and SCIA-MACHY) implied that emissions were too low by $\sim 55\%$ in South America, by $\sim 85\%$ in southern Africa, and by $\sim 40\%$ in northern Africa. The underestimates were largely in the biomass burning season and were attributed to deficiencies in the GFED2 inventory. It is important to note that in the tropics their results depended on which satellite data were used. Chevallier et al. (2009) also found that GFED2 emissions from Africa are too low in an inverse study using MOPITT data and the LMDZ-INCA model, but to a lesser extent than Kopacz et al. (2010).

Another distinctive discrepancy between the models and observations is the overestimate of CO in the eastern tropical Pacific within the Inter-tropical Convergence Zone (ITCZ),

mainly in August and September. This discrepancy is larger in GEOS-4 than in GEOS-5, and is larger in 2005 than in 2006, when emissions of CO from fires over South America were much lower than in 2005 (Fig. 1). The model overestimate extends to the central Pacific, as shown by the comparison at Christmas Island (2° N, 157° W) in Fig. 2.

Seasonal burning starts in northern Africa in November, and it causes the maximum in December and January over the northeastern equatorial Atlantic. In January 2006, the models underestimate CO in the vicinity of the fires in West Africa, and overestimate CO over a small region in equatorial Africa.

The very high CO over Indonesia and the eastern Indian Ocean in 2006 was caused by increased biomass burning associated with a drought induced by El Niño and the Indian Ocean Dipole (e.g. Logan et al., 2008; Rinsland et al., 2008; Nassar et al., 2009). A model analysis of the TES observations in this region in late 2006 using the GEOS-Chem model driven by GEOS-4 is given by Nassar et al. (2009).

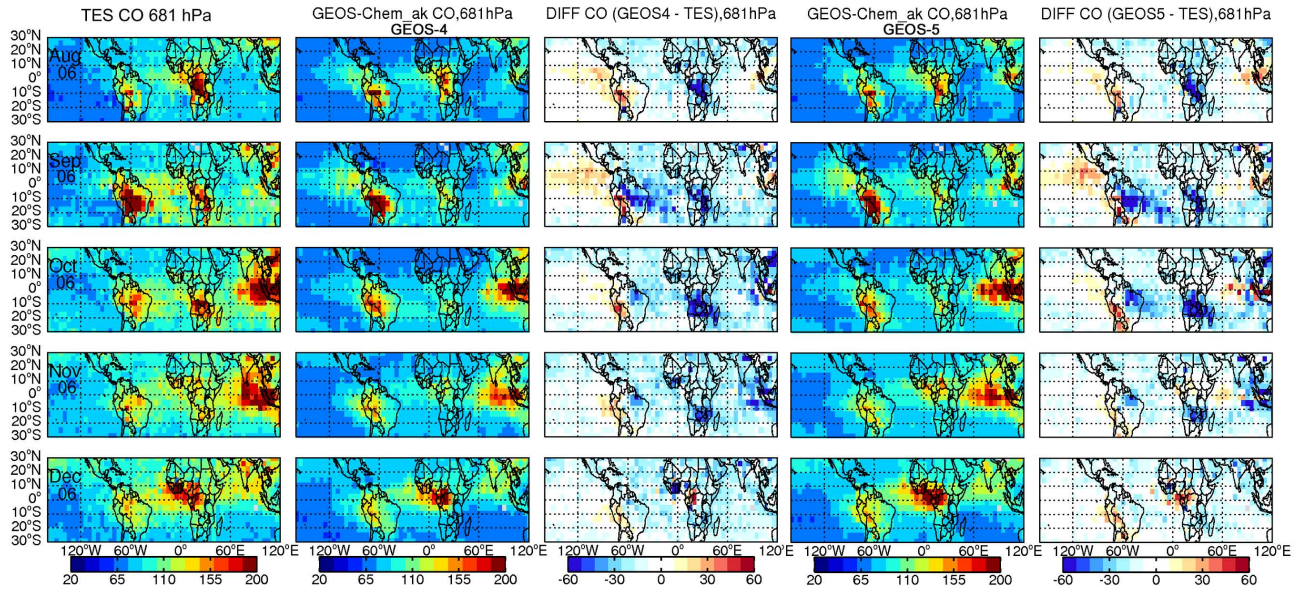


Fig. 4. Lower tropospheric CO at 681 hPa from August 2006 to December 2006 from TES (left column), the GEOS-4 model, and the difference (model wAK–TES) (2nd and 3rd columns), the GEOS-5 model, and the difference (model wAK–TES) (4th and 5th columns).

4.2 Upper troposphere

Figures 5 and 6 compare the spatial pattern of CO at 215 hPa from the MLS data to the GEOS-4 and GEOS-5 model results. We show MLS at 215 hPa as it is close to the level of maximum convective detrainment (Folkins and Martin, 2005; Fueglistaler et al., 2009). The color bar range for MLS CO is twice of that for model results because of the factor of two high bias in the MLS retrieval at 215 hPa noted above (Livesey et al., 2008).

The GEOS-4 model shows a prominent maximum over the eastern tropical Pacific in August and September of 2005 that is not present in the MLS observations. This maximum is collocated with the overestimate of CO in the LT (Fig. 3). There is a similar, although much weaker, maximum in the GEOS-5 results for 2005, and a much weaker feature in both 2006 simulations.

Over South America, MLS CO reaches its seasonal maximum in October in 2005 and in September in 2006. The model CO maximum with GEOS-4 occurs about 1 month late in both years, and it persists until December in 2006. With GEOS-5, the model maximum occurs 1–2 months late in 2005 and 3 months late in 2006. We explore the causes of these discrepancies in Sect. 5.

Over southern Africa, MLS CO is highest in September and October of 2005 and in August to October of 2006, with a similar pattern in the two models. This is seen more clearly in the regional time series discussed below. Both models show a maximum in CO over the Gulf of Guinea, Nigeria, and Cameroon in November to January that is not apparent in the observations. This maximum persists into March in

the models, but appears in the observations only in February and March, where it is a relatively weak feature.

Both models show a similar spatial pattern to MLS for the high CO over Indonesia and the Indian Ocean as it builds up from September to November in 2006, and disappears in December. This was also shown in Nassar et al. (2009) using TES data for the lower and upper troposphere. Transport of fire emissions to the UT in August are obvious in the GEOS-4 simulation, but are much less apparent in the MLS data and in the GEOS-5 simulation. Neither simulation shows the prominent maximum in MLS CO over northern India in August that is associated with the Indian monsoon as discussed in the Introduction, and as reported in MOPITT data in Kar et al. (2004).

5 Influence of dynamics

The spatial and vertical distribution of CO in and near the source regions depends on the position of strong vertical mixing relative to the source distribution at lower altitudes, as well as the influence of horizontal transport by the prevailing winds.

In this section, we examine the influence of transport on CO in the two simulations based on the results for the four major biomass burning regions and for the eastern Pacific, where there is a major discrepancy with the observations as shown in Fig. 7. We interpret the satellite data with the GEOS-Chem model and identify possible causes for the discrepancies between model simulations and observations. Furthermore, we use the satellite data to evaluate the effect of different convective parameterizations in GEOS-4

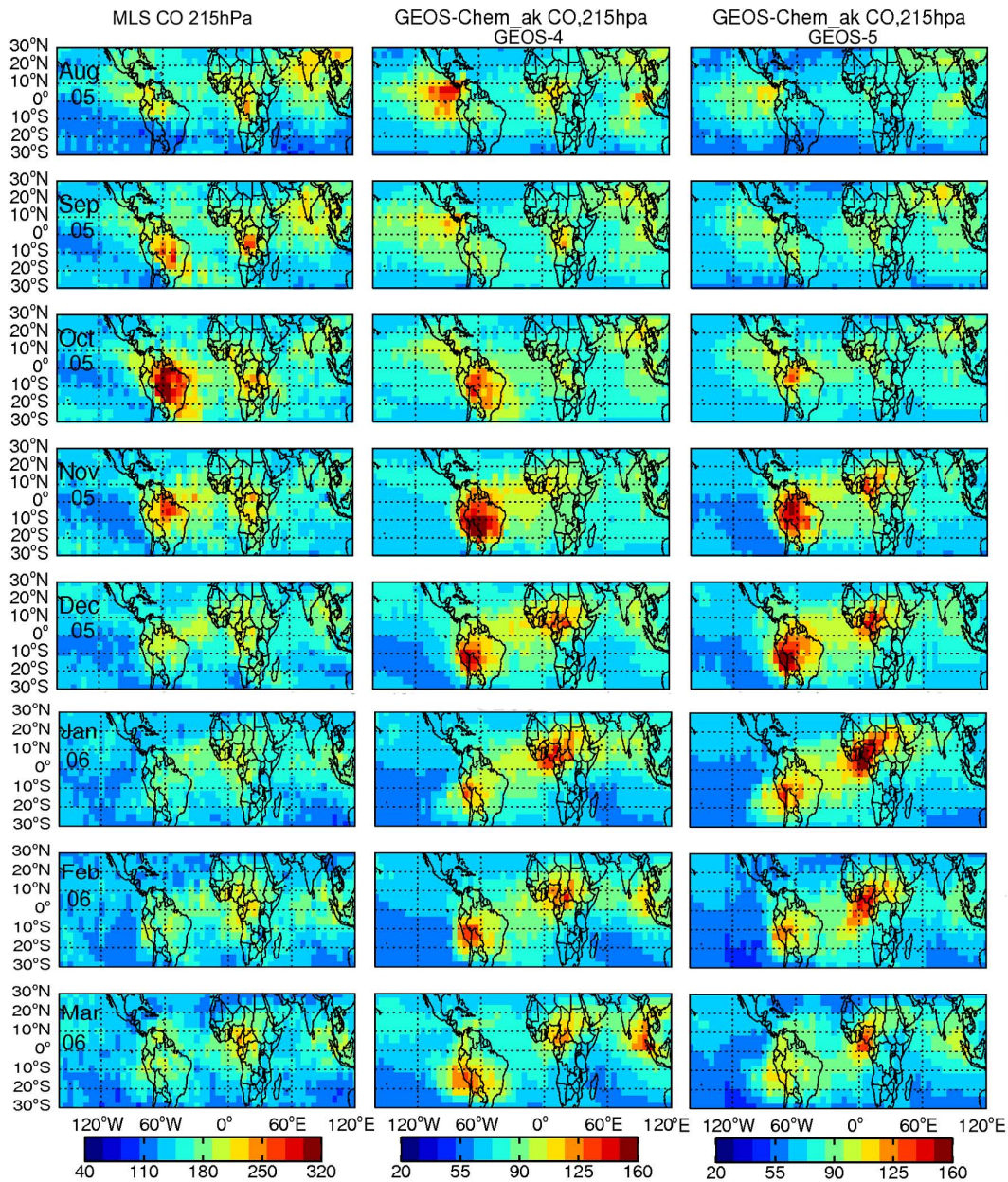


Fig. 5. Upper tropospheric CO at 215 hPa from August 2005 to March 2006 from MLS (left), the simulations driven by GEOS-4 (middle) and GEOS-5 (right) with the MLS AKs applied. The color bar range of MLS is twice of that of model results because of the factor of two high bias of the MLS retrieval at 215 hPa (Livesey et al. 2008). Difference plots are not shown because of concern over the absolute accuracy of the CO retrieval.

and GEOS-5 on model performance. Tagged CO simulations are also used to investigate the causes of these discrepancies. This approach allows us to characterize important aspects of transport in the GEOS-4 and GEOS-5 meteorological fields, and to determine deficiencies in the CO sources.

5.1 South America

The left column of Fig. 8 shows observed and modeled time series over South America at the two levels shown in Figs. 3–6, as well as comparisons with TES at an intermediate level, 422 hPa, and with MLS at 147 hPa. The figure includes model results at each level with and without application of the averaging kernels.

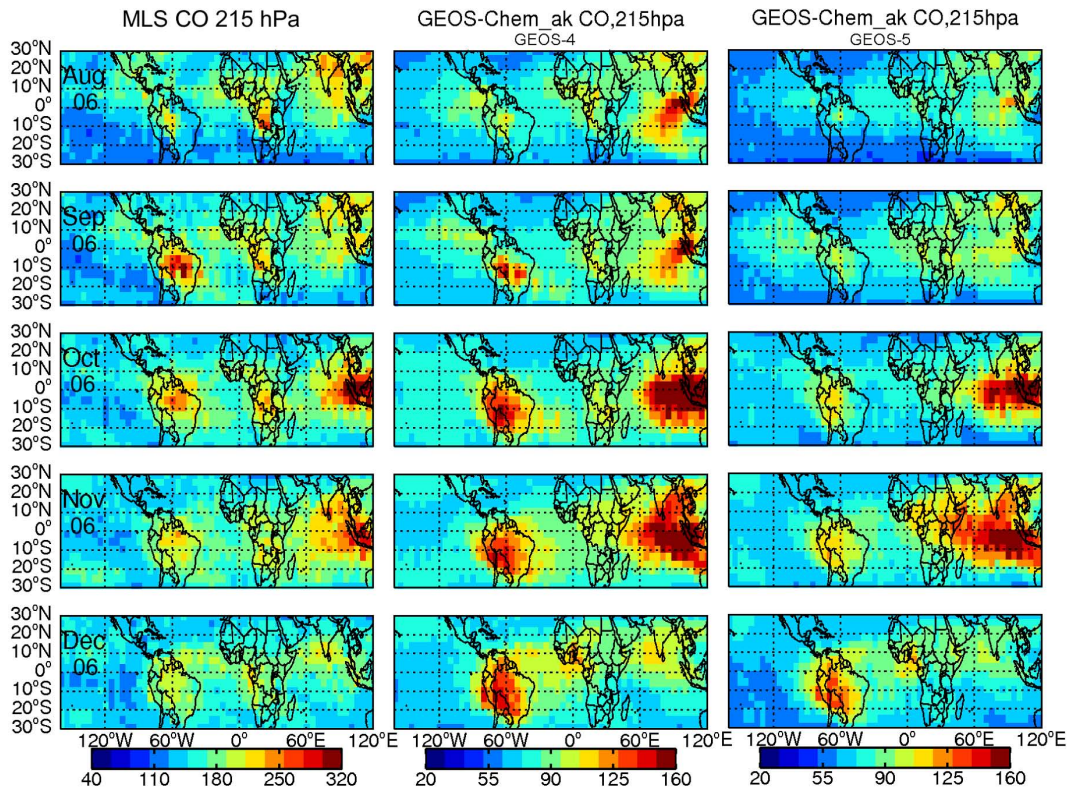


Fig. 6. Upper tropospheric CO at level 215 hPa from August to December 2006 from MLS (left), the simulations driven by GEOS-4 (middle) and GEOS-5 (right) with the MLS AKs applied. See Fig. 5 for further details.

Application of the AK to the model results makes a particularly large difference at 681 hPa before the TES bench warm-up in late November 2005. This is caused by the large effect of the prior information, because of the low sensitivity of TES at the lower altitudes with low DOFs at that time. TES has a higher sensitivity in the middle troposphere ($\sim 400\text{--}500$ hPa) than in the lowest part of the troposphere (e.g. Luo et al., 2007a). Application of the MLS AKs modifies the model results very little.

Over South America, in both GEOS-4 and GEOS-5, CO is highest at 681 hPa in August and September 2005, the months with peak biomass burning emissions. Application of the TES AKs delays the peak to September–October for GEOS-4, a consequence of the sensitivity of TES to CO at higher altitudes, where CO peaks later (see panel for 422 hPa). GEOS-4 CO is highest in September and October at 422 hPa and in September in 2006, matching the timing of the TES data. However, the GEOS-4 maximum in CO at 215 and 147 hPa is clearly a month late compared to the MLS data, and in 2006, the model peak stays high for too long. Application of the TES AKs to GEOS-5 at 681 hPa induces too broad a maximum, again a consequence of the sensitivity of TES to CO at higher altitudes. The CO peak at 422 hPa in GEOS-5 is broader and 1–2 months later than that for GEOS-4 in 2005, and in both years, the underestimate of

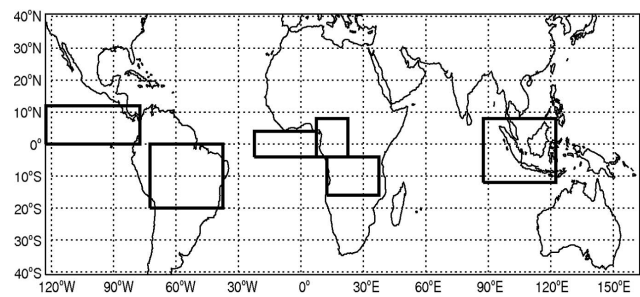


Fig. 7. Location of the regions discussed in this study. From left to right: East Pacific ($0^{\circ}\text{--}12^{\circ}$ N, 122.5° W– 77.5° W), South America ($0^{\circ}\text{--}20^{\circ}$ S, 72.5° W– 37.5° W), Gulf of Guinea (4° S– 4° N, 22.5° W– 7.5° E), northern Africa (4° S– 8° N, 7.5° E– 22.5° E), southern Africa (16° S– 4° S, 12.5° E– 37.5° E) and Indonesia (12° S– 8° N, 87.5° E– 122.5° E).

TES data is larger for GEOS-5 than for GEOS-4. At 215 hPa the GEOS-5 CO maximum is 1–2 months late in 2005, and 3 months late in 2006.

Figure 9 shows the seasonal variation of spatial patterns of the vertical air mass flux, which is closely related to the seasonal variation of ITCZ, superimposed on the CO mixing ratio. Results are shown from the LT to UT in GEOS-4 in 2005.

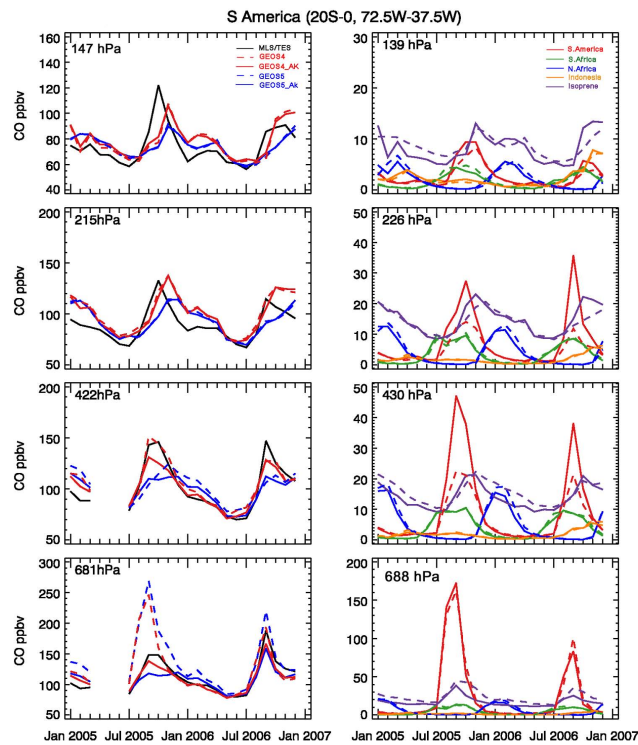


Fig. 8. Left: Time series of TES CO (681 and 422 hPa) and MLS CO (215 and 147 hPa) (black) and model results for GEOS-4 (red) and GEOS-5 (blue) over South America. The MLS CO values at 215 hPa have been scaled by 0.5 and those at 147 hPa by 0.7, based on the validation shown in Livesey et al. (2008). Solid lines show the model results with the AKs applied, dashed lines show the model results without the AKs. Right: Time series of tagged CO tracers over South America from individual sources: biomass burning in South America (red), southern Africa (green), northern Africa (blue) and Indonesia (orange), and the biogenic source from isoprene (purple). Results are shown for GEOS-4 (solid lines) and GEOS-5 (dashed lines) at model levels 688, 430, 226, and 139 hPa.

During the boreal summer the ITCZ is located at its northernmost location north of the Equator. The ITCZ then shifts southwards, and deep convection moves over South America in October, reaching about 30° S, and intensifies into austral summer (Manabe et al., 1974; Fu et al., 2001; Panarello and Dapena, 2009). Fu et al. (1999) suggests that the onset of wet season over the South America starts around October, induced by the systematic buildup of planetary boundary layer (PBL) moisture, with the release of the latent heat flux. This behavior is seen in the maps of vertical mass flux in Fig. 9, and maps of the convective mass flux alone have similar spatial patterns (not shown). The timing of the CO maximum changes from September at 688 hPa to October at 430 hPa and to November at 226 hPa, following the southward migration of the upward mass flux.

GEOS-5 has a relatively slow and gradual southward migration of the upward mass flux from August to December

(Fig. 10). In contrast to GEOS-4, the migration is limited to the equatorial region in October in the UT, and most of the burning region lacks deep vertical mixing to transport surface emissions to the upper levels. Thus, although the seasonal CO maximum appears in October at 430 hPa as it does in GEOS-4, CO is much lower. At 226 hPa, the GEOS-5 model maximum in November is considerably smaller than that in GEOS-4, and the GEOS-5 CO is higher in December than in November.

Figure 11 shows the vertical profiles of mass flux associated with convection and large scale advection over South America in GEOS-4 and GEOS-5 from August to December in 2005. In GEOS-4 the convective mass flux increases substantially between September and October, with a similar increase in the total mass flux. However, in GEOS-5 both the convective and total mass fluxes increase more gradually in this period. The convective mass fluxes over South America in both GEOS-4 and GEOS-5 are extremely small by 200 hPa, and the GEOS-5 mass fluxes peak at lower altitudes than those of GEOS-4. Figure 11 implies that the dominant mechanism for vertical transport near 215 hPa in both GEOS-4 and GEOS-5 is large-scale vertical advection rather than convection. The fact that convection detrains at too low an altitude likely contributes to the one-month lag of the UT CO maximum in the model simulations compared to the observations (Figs. 3–6). Compared to GEOS-4, the convective mass flux in GEOS-5 decays more quickly with increasing altitude, thus mixing by slow advection plays more of a role. The lag in GEOS-5 is greater in part because convection decays at a lower altitude, and in part because convection moves southward later than in GEOS-4.

In 2005 the observed CO maximum occurs one month later at 215 hPa than at 681 hPa, while in 2006, the observed CO maximum occurs in September from 681 hPa to 215 hPa, implying stronger vertical mixing in 2006 than in 2005. Convection may have been weaker in 2005 because of the warmer sea surface temperatures in the north tropical Atlantic (Marengo et al., 2008; Zeng et al., 2008).

We examined source attribution of CO in the UT using a tagged CO simulation. Figure 8 (right column) shows time series of tagged CO tracers from individual sources, including biomass burning sources from South America, southern Africa, northern Africa and Indonesia, and the biogenic source from isoprene over South America, for GEOS-4 (solid lines) and GEOS-5 (dashed lines). In the LT, CO from local biomass burning dominates over South America from August to October in 2005, and to September in 2006. In the MT and UT, with GEOS-4, the local biomass burning contribution dominates from August to October in 2005, and in August and September in 2006, after which it is exceeded by the contribution from isoprene oxidation. As the wet season progresses southward over the continent, fires are extinguished (Fig. 1) and vertical mixing increases rapidly, as shown above. However, the source of CO from isoprene oxidation persists throughout the year, and thus its influence on

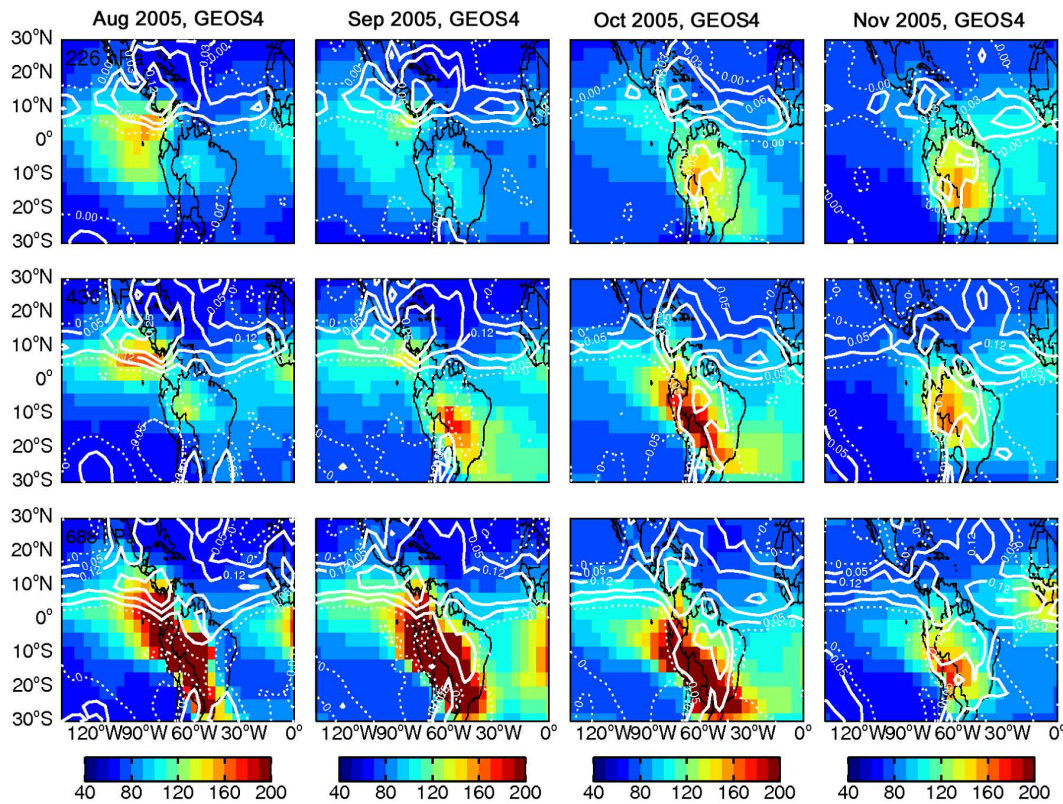


Fig. 9. Spatial patterns of the vertical air mass flux (Pa s^{-1}) superimposed on the CO mixing ratio (colors, in ppb) from August to December 2005 at 688 (bottom), 430, and 226 (top) hPa in the model driven by GEOS-4. The contour levels are: $(-0.05, 0, 0.05, 0.12, 0.2)$ for 688 and 430 hPa and $(-0.05, 0, 0.03, 0.06, 0.12)$ for 226 hPa. Positive values are upward fluxes (solid lines), negative values are downward fluxes (dashed lines).

CO in the UT increases and becomes dominant from November onwards (and December in GEOS-5) as the upward air mass flux increases from month to month.

In the GEOS-5 simulation, much less CO from biomass burning is transported to the MT and UT because of weaker vertical mixing. The CO source from isoprene is similar to that from biomass burning in the MT, and exceeds it in the UT, providing the dominant contribution to the seasonal maximum that persists into December in 2005, and does not occur until December in 2006. Clearly, deficiencies in sources of CO, as well as in vertical transport, contribute to the discrepancies in the timing of model at 215 hPa over South America.

There is a weak secondary maximum in CO over South America in the UT in February to April 2006. The tagged runs show that CO from biomass burning in northern Africa contributes significantly to this feature, with the remainder from isoprene oxidation. In the UT, the isoprene source of CO includes transport of emissions from Africa.

We note that CO in the tagged simulation does not exactly match CO in the on-line chemistry simulation, because the treatment of the source of CO from isoprene (and other hydrocarbons) is necessarily simplified, and it is treated as a

direct CO source (Duncan et al., 2007). In the on-line simulation, CO is produced from degradation products of isoprene oxidation. Nevertheless, the tagged runs give very useful information on source apportionment, and aid in understanding the results shown in Fig. 8 (left column).

The comparison of TES and model CO in the LT (Figs. 3–4) show that model CO is too low in eastern Brazil, where biomass burning is a major source, but CO is somewhat high in western South America where the isoprene emissions are highest, as shown in Fig. 13. These discrepancies of the spatial pattern of CO over South America are caused by an underestimate of emissions from biomass burning (Kopacz et al., 2010), and we infer that the overestimate in the west of the continent is caused by an overestimate of isoprene emissions. The simulated CO using the PECCA algorithm is on average 5% (5–10 ppb) lower than the standard runs using the hybrid algorithm. However, this decrease is not enough to counteract the overestimate of isoprene emissions in our model.

The discrepancy in the timing of the CO maximum at 215 hPa could also be influenced by the underestimate in the GFED2 biomass burning emissions implied by the inversion study of CO sources (Kopacz et al., 2010). As noted above,

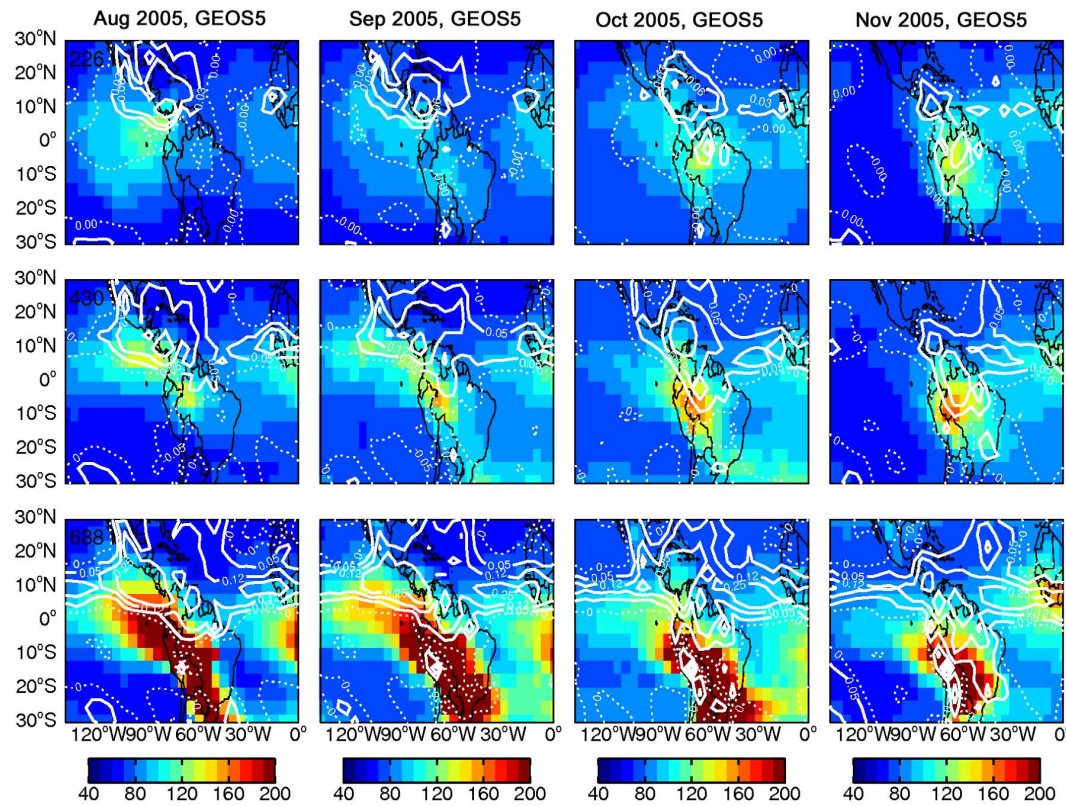


Fig. 10. Spatial patterns of the vertical air mass flux (contours in Pa s^{-1}) superimposed on the CO mixing ratio (colors, in ppb) from August to December 2005 in the model driven by GEOS-5. See Fig. 9 for further details.

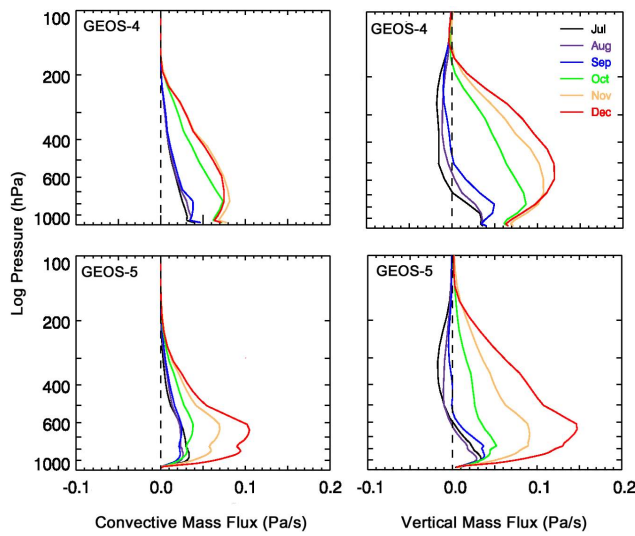


Fig. 11. Vertical profiles of convective air mass flux (left) and the total air mass flux (right, sum of convection and advection) in South America from August to December 2005. The top panels are for the model driven by GEOS-4 and the bottom panels are for the model driven by GEOS-5.

Kopacz et al. (2010) found that CO emissions were too low by 55% in South America, by 85% in southern Africa, and by $\sim 40\%$ in northern Africa. However, their simulations with a posteriori sources led to overestimates of CO over northern Africa when compared to SCIAMACHY and MOPITT data, and to MOZAIC data in November to February. We conducted a sensitivity study where we multiplied the CO emissions by monthly scaling factors from Kopacz et al. (2010) at each grid from the results of the inversion study only over South America and southern Africa. The scaling factors vary seasonally, with maxima in September and October over southern Africa and in October over South America. Results for GEOS-4 show that modeled CO with increased emissions is somewhat high from 681 hPa to 215 hPa in July to November, with the biggest increase in October as shown in Fig. 14. For GEOS-5, the simulation with increased emissions agrees well with TES data in the LT and MT. We caution, however, that the scaling factors are from an inversion using GEOS-4 meteorological fields, and the better agreement with GEOS-5 may be fortuitous. The discrepancy in the timing of the seasonal maximum between both models and observations remains at 215 hPa and 147 hPa. As might be expected, the higher emissions exacerbate the problem of excessively high CO over the eastern tropical Pacific in July to September, and over the Andes, although the model matches CO over eastern

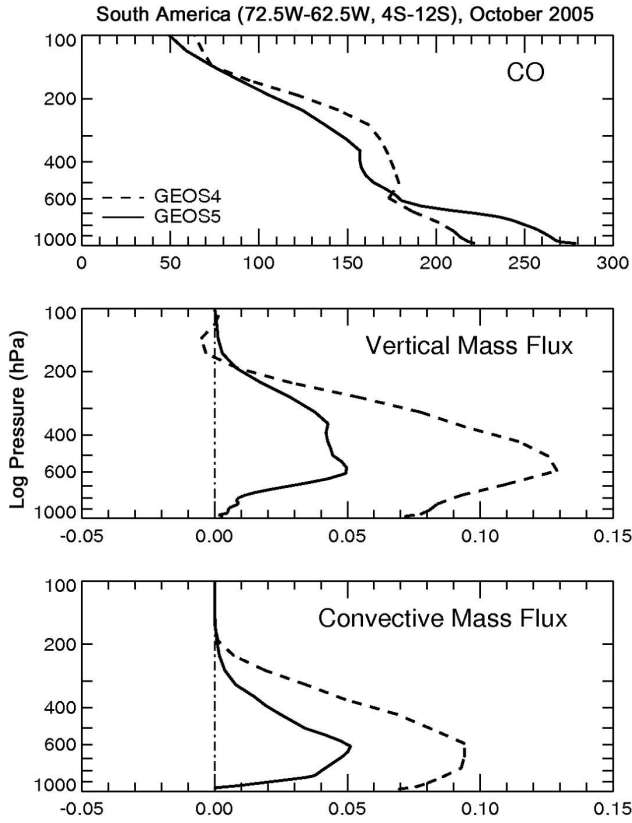


Fig. 12. Vertical profiles of CO (top), total air mass flux (middle), and convective mass flux (bottom) in October 2005 at the center of the biomass burning region in South America (72.5° W– 62.5° W, 4° S– 12° S) for simulations driven by GEOS-4 (dashed) and GEOS-5 (solid). Mass flux is in Pa s^{-1} , CO is in ppb.

Brazil (Fig. 15). This was also found in the a posteriori simulations of Kopacz et al. (2010), compared to MOPITT data.

5.2 East Pacific

As shown in Figs. 3 and 4, both GEOS-4 and GEOS-5 overestimate CO over the East Pacific region in August and September. The overestimate is worse in 2005 due to much higher emissions in South America. In the UT, the overestimate in August 2005 persists over the East Pacific, particularly north of the equator where deep convection is located, in the model with GEOS-4, but it is less of a problem in GEOS-5. In September 2005, model CO with both GEOS-4 and GEOS-5 is higher over the Eastern Pacific than over South America, while the MLS data show a maximum over the continent.

The bi-polar pattern with overestimates over the East Pacific and underestimates over South America in both the model simulations in August 2005 in the LT suggests that the south-easterly winds blowing from the burning region of South America may be too strong in both GEOS-5 and

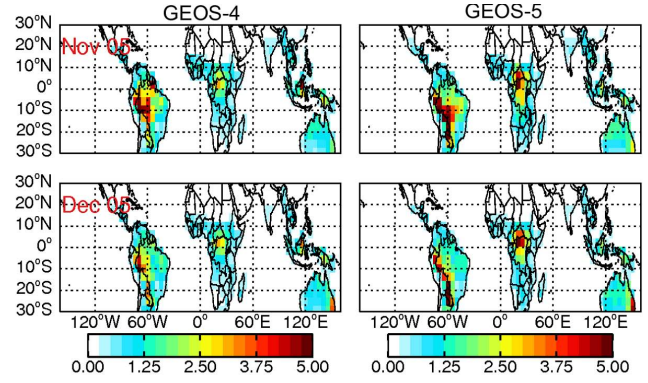


Fig. 13. Isoprene emissions (10^{12} atoms $\text{C cm}^{-2} \text{ s}^{-1}$) in November (top) and December (bottom) 2005 in the model driven by GEOS-4 (left) and GEOS-5 (right).

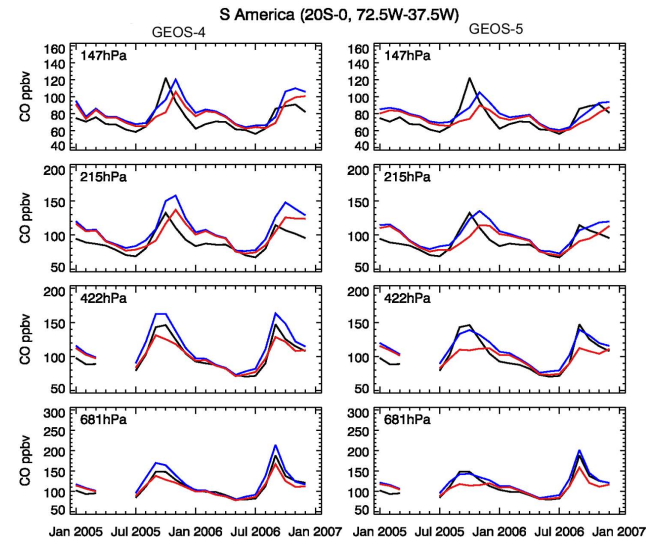


Fig. 14. Time series of TES CO (681 and 422 hPa) and MLS CO (215 and 147 hPa), scaled as in Fig. 8 (black) with (left) GEOS-4, (right) GEOS-5 model results over South America. The standard simulation is in red, and the simulation with adjusted emissions (see text) is in blue.

GEOS-4, transporting too much CO to the east Pacific where it is lofted to the UT in the ITCZ.

Figure 16 shows that the profiles of vertical mixing over the East Pacific are substantially different in GEOS-5 and GEOS-4. The upward mass flux is larger in GEOS-4 than in GEOS-5 from about 600 to 300 hPa, and the CO in GEOS-4 exceeds that in GEOS-5 from about 500 to 200 hPa as a consequence.

5.3 Africa

The dominant meteorological features in the troposphere over Africa include the seasonal migration of the ITCZ, the Harmattan flow, the African Easterly Jet (AEJ) (e.g.,

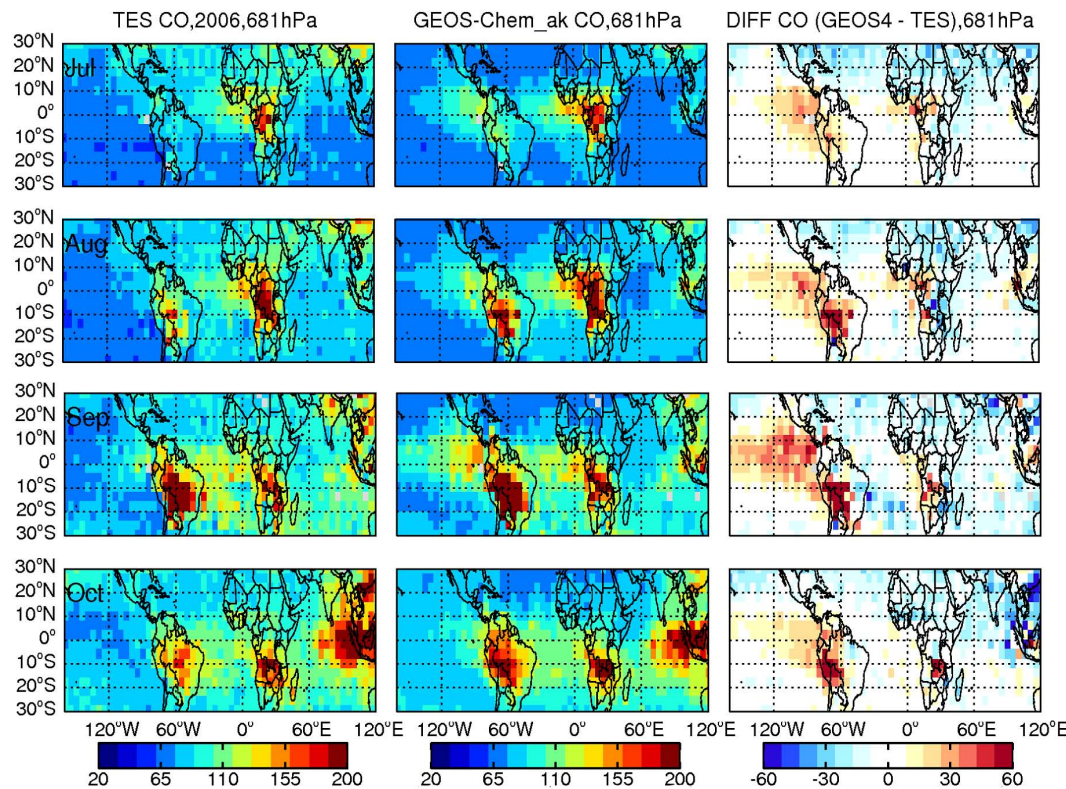


Fig. 15. Lower tropospheric CO at 681 hPa from July to October 2006 from TES (left), the GEOS-4 simulation with modified emissions with the TES AKs applied (center), and the difference (modified model wAK–TES) (right).

Thorncroft and Blackburn, 1999) and the trade winds. These features have a complex influence on the redistribution of CO from its biomass burning region in the respective winter seasons of the two hemispheres, as discussed below.

5.3.1 Southern Africa

Over southern Africa, the model simulations are lower than observations, because of the low surface emissions in the model. The model simulations driven by both GEOS-4 and GEOS-5 match the phase of the observed CO variation from 681 to 215 hPa fairly well, although the magnitude of the maximum is underestimated considerably (Fig. 17). Both simulations and observations show a time lag between the peak in fire emissions (July and August) and in CO (September and October), as observed in Edwards et al. (2006) using MOPPIT CO and MODIS fire count data. They conjectured that the lag might be caused by smoldering fires at the end of burning season. We address the reasons for the lag below, after an analysis of the prevailing meteorology. To illustrate the pathway of CO-laden air we show in Fig. 18 its distribution along with the wind fields and vertical air mass flux in August and September of 2005, a year with a typical summer monsoon pattern. Southeasterly trade winds prevail over southern Africa at lower altitudes, and transport CO from the fires to the Gulf of Guinea. The low-level monsoon westerlies and

the north-easterly Harmattan winds converge between 10° N and 15° N, where the ITCZ is located. The Harmattan winds become stronger and move equatorward near 700 hPa, and merge with the southeasterly trade winds around 5° N. There is a region of strong upward mass fluxes in the MT (430 hPa) primarily north of the Equator that loft CO from the fires to the MT and UT. Several studies discuss these transport pathways during the West Africa monsoon season, in the context of interpreting ozone and CO observations (Sauvage et al., 2005, 2007a), including MLS CO data (Barret et al., 2008, 2010). Barret et al. (2008) attribute the CO maximum over northern Africa at 215 hPa (in July 2006) mainly to convective uplift of CO-rich air from biomass burning in southern Africa following these transport pathways. A continental anticyclone develops over the region of the fires in southern Africa and a mid-tropospheric cap persists as a result of the subsiding air at the center of the anticyclone, inhibiting the development of convection beneath (Fig. 18) (Karoly and Vincent, 1998). Thus in August (and also in July), a large amount of CO is trapped in the LT over southern Africa, while in the MT and UT, a CO maximum appears to the north of the Equator over the continent where it is lofted in the ITCZ. A similar CO maximum is evident in the MLS data at 215 hPa in 2005, except it is slightly south of the equator (Fig. 5).

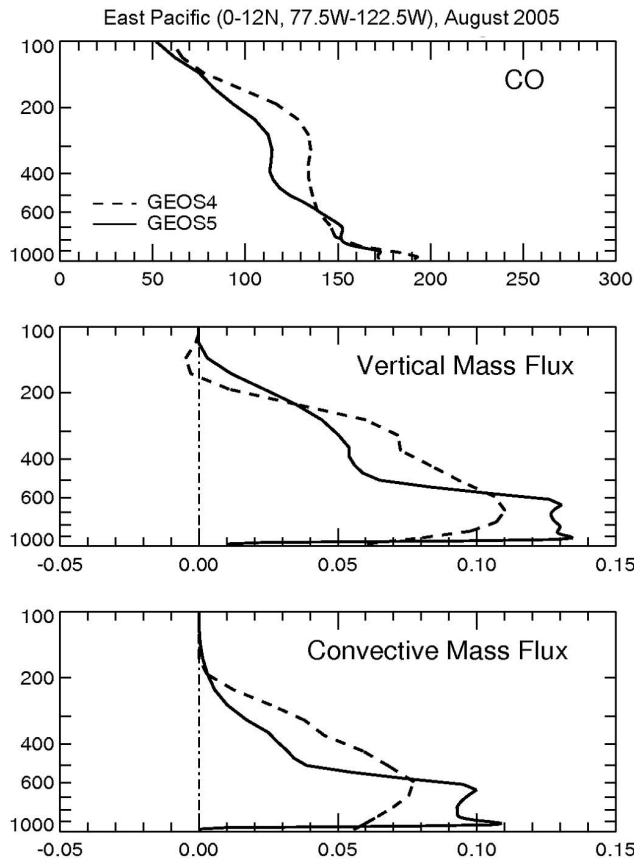


Fig. 16. Vertical profiles of CO (top), total vertical mass flux (middle), and convective mass flux (bottom) in August 2005 over the East Pacific (0° – 12° N, 77.5° W– 122.5° W) for simulations driven by GEOS-4 (dashed) and GEOS-5 (solid). Mass flux is in Pa s^{-1} , CO is in ppb.

In September 2005, with the southward shift of the ITCZ, the region with upward mass flux propagates south in the MT, bringing more CO to the higher altitudes south of the Equator. Meanwhile, with the northwest propagation of the continental anticyclone, recirculation of CO over central Africa occurs between 0 and 10° S, contributing to the high CO south of the equator in the UT as observed in the MLS data (Fig. 5). In October, the region with strong upward mass flux migrates to southern Africa, lofting the remaining high CO from the fires, which are mostly extinguished. The tagged CO runs show that transport from South America by subtropical westerlies in the MT and UT also contributes to the CO maximum in September and October (Fig. 17, right column). Returning to the question of the delay in the CO maximum compared to the earlier peak in emissions, we argue that it is caused by the factors discussed above. First, subsidence over southern Africa allows CO to build up in the LT until convection moves south starting in September. Secondly, TES (and MOPITT) retrievals at ~ 700 hPa have broad averaging kernels, extending into the MT, and sensitivity

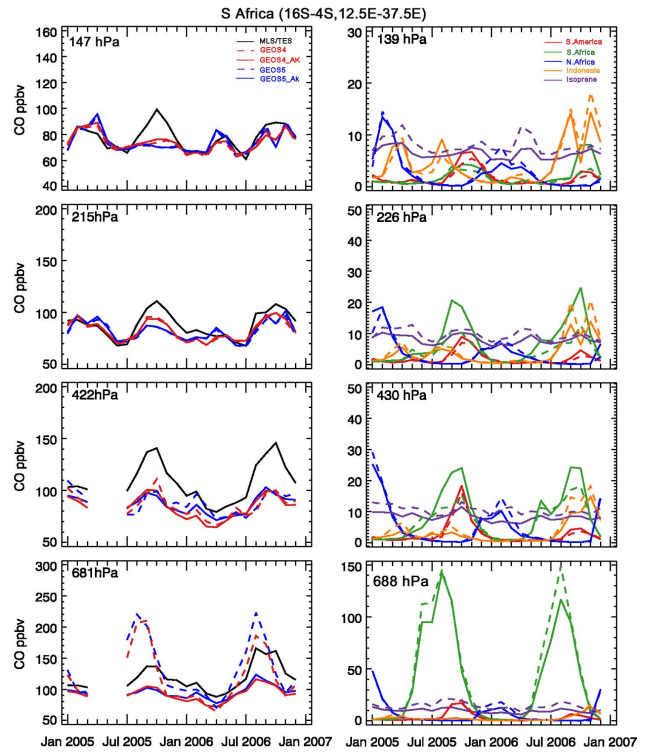


Fig. 17. Left: Time series of TES CO (681 and 422 hPa) and MLS CO (215 and 147 hPa, scaled as in Fig. 8) (black) and model results for GEOS-4 (red) and GEOS-5 (blue) over southern Africa. Solid lines show the model results with the AKs applied, dashed lines show the model results without the AKs. Right: Time series of tagged CO tracers over southern Africa from individual sources: biomass burning in South America (red), southern Africa (green), northern Africa (blue) and Indonesia (orange), and the biogenic source from isoprene (purple).

is relatively low at the surface (~ 900 hPa over the African plateau). The maximum in the MT is 1–2 months later than that at 700 hPa, because of the delay in lofting of African emissions, combined with the maximum in transport of fire emissions from South America in October (Fig. 17). The influence of CO in the MT on the retrieval at 700 hPa contributes to the delay in the satellite CO in the LT relative to the peak in the emissions. Figure 19 shows the mean vertical mass fluxes over southern Africa. There is subsidence to a lower level in September and October in GEOS-5 than in GEOS-4 in 2005. The region of upward air mass flux has moved further south in GEOS-4 than in GEOS-5 in September (not shown), and as a result of differences in the spatial pattern and the stronger upward fluxes of air in GEOS-4, more CO is lofted to the MT and UT in GEOS-4 than in GEOS-5. This is responsible for the lower CO in the UT in the GEOS-5 simulation compared to that with GEOS-4 (Fig. 5).

The situation is more complex in 2006, an El Niño year with very high fire emissions from Indonesia that are

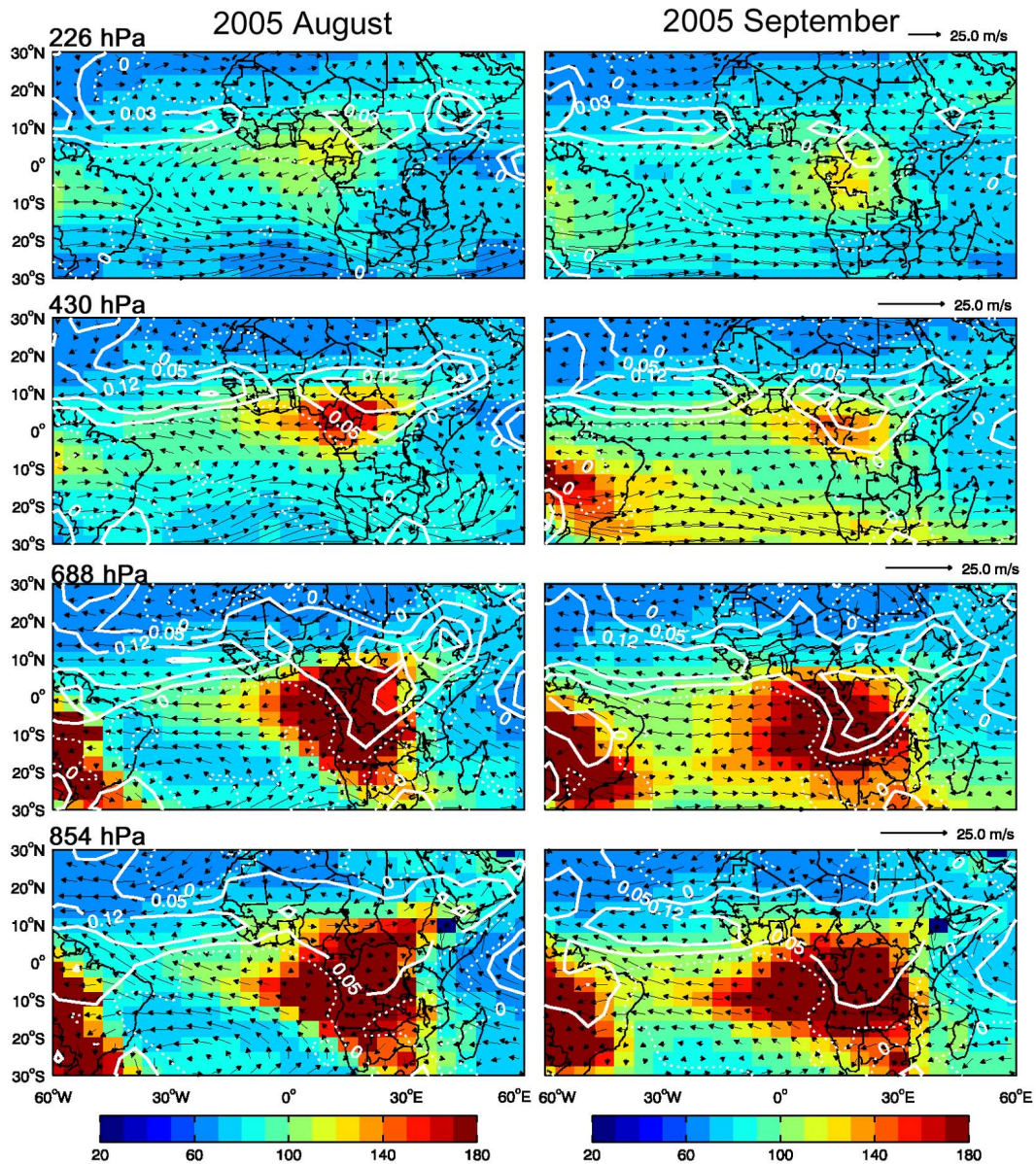


Fig. 18. CO mixing ratio (ppb) overlaid with horizontal wind vectors in August (left) and September (right) 2005 at 854, 688, 430, and 226 hPa for the GEOS-4 model. The vertical air mass flux (Pa s^{-1}) is shown by contours: $(-0.05, 0, 0.05, 0.12, 0.2)$ for 854, 688, and 430 hPa, and $(-0.05, 0, 0.03, 0.06, 0.12)$ for 226 hPa. Positive values are upward fluxes (solid lines), negative values are downward fluxes (dashed).

transported westwards towards Africa (Figs. 4 and 6). There is a broad CO maximum from August to October in the LT and MT that extends into November in the UT over southern Africa (Fig. 17, left column). The tagged CO runs show that transport of the emissions from Indonesia provides a significant contribution to the peak over Africa in September to November, exceeding the contribution from Africa itself in the UT in GEOS-5. The relative minimum in this contribution in October reflects changes in the winds over the Indian Ocean in that month (not shown). By 147 hPa, emissions from Indonesia are the dominant contribution to the peak

in September in both GEOS-4 and GEOS-5. The upward air mass flux over Africa is higher in 2006 than in 2005 in October (Fig. 19), while the contribution from South American emissions is lower (Fig. 17, right column), so there is not much interannual variation of CO in the UT.

The tagged runs show that the secondary maximum in January to February in the LT and MT is caused by fire emissions from North Africa. The later maximum in the UT (February to April) is also from North African fires, with a significant contribution from fires in Indonesia in 2005. Model CO is systematically low in the LT and MT outside the southern

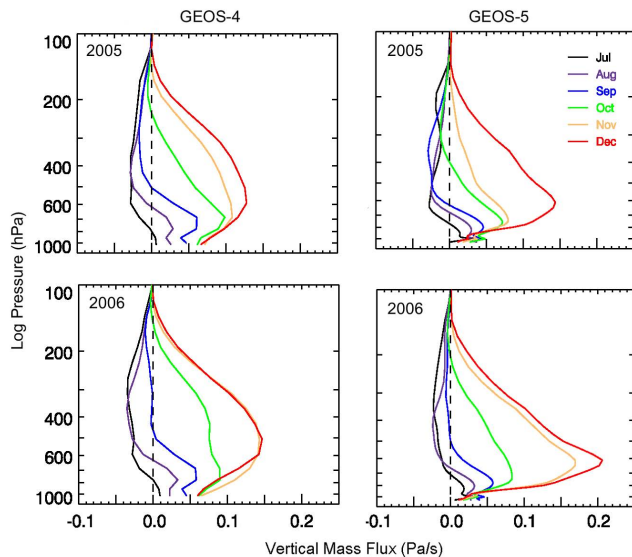


Fig. 19. Vertical profiles of total air mass flux (convection and advection) in southern Africa from August to December in 2005 (top) and 2006 (bottom). The left panels are for GEOS-4 and the right panels are for GEOS-5.

burning season, particularly in the GEOS-4 simulation (by $\sim 10\text{--}25$ ppb).

The GEOS-4 simulation with increased emissions improves agreement with observed CO in the LT and MT in July to October, as shown in Fig. 20 (left). However, CO is too high at 215 hPa in September and October. The difficulty of matching CO in both the LT and UT suggests that convection may detrain at too high an altitude over Africa in GEOS-4 in these months. The GEOS-5 simulation with increased emissions provides better agreement with observed CO from the LT to UT, especially at 215 hPa (Fig. 20, right). As discussed above, convection in GEOS-5 ends at a lower altitude than that in GEOS-4. Over southern Africa, vertical mixing in GEOS-5 may be more realistic, with the discrepancies between model and observations caused primarily by deficiencies in the GFED2 emissions.

5.3.2 Northern Africa

Over northern Africa, the observed CO has a biannual pattern, with the primary CO maximum occurring in boreal winter and a secondary maximum in summer (Fig. 21). Both GEOS-4 and GEOS-5 match the phase and magnitude of the CO variation from 681 to 422 hPa fairly well. The models also have a high bias of $\sim 20\%$ in early 2005 in the LT and MT, during the burning season. At 215 hPa, MLS does not show a strong seasonal cycle, while it is pronounced in the models. There is a deep early summer minimum at 215 hPa in the GEOS-5 simulation, less so in the GEOS-4 results. At the upper level, 147 hPa, the models and MLS data are again

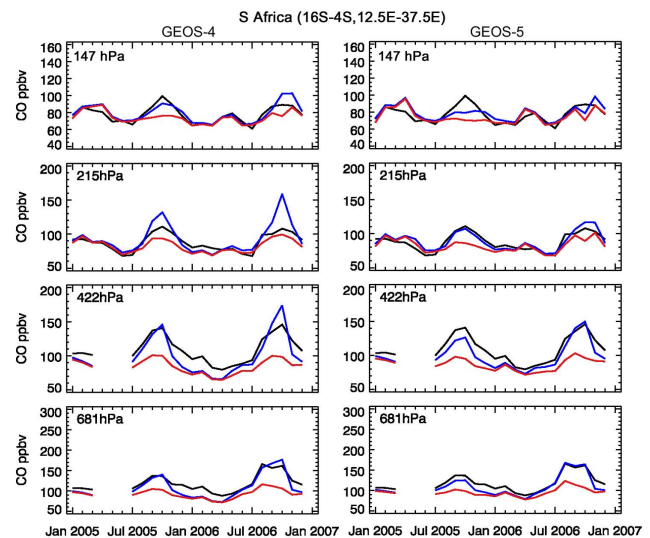


Fig. 20. Time series of TES CO (681 and 422 hPa) and MLS CO (215 and 147 hPa, scaled as in Fig. 8) (black) with (left) GEOS-4, (right) GEOS-5 model results over southern Africa. The standard simulation is in red, and the simulation with adjusted emissions (see text) is in blue.

in reasonable agreement, with a more prominent seasonal cycle in the data and models.

Aircraft data from West Africa allow independent evaluation of the CO profile at the peak of the burning season. Figure 22 shows CO vertical profiles over Lagos (6°N , 3°E) from the MOZAIC program (Nedelec et al., 2003; Barret et al., 2008; Williams et al., 2009). The data are primarily for 2002–2004, and are compared to the mean of the model for 2005 and 2006. Despite the different years represented by the observations and model, both CO profiles exhibit a dramatic decrease between 800 and 600 hPa, particularly in December and January. GEOS-5 gives a better simulation than GEOS-4 of the high CO in the boundary layer. However, model CO is too high from 500 to 200 hPa by about 25% (GEOS-4) and 40% (GEOS-5) in January, and much too low in boundary layer. The transport patterns in the model suggest that the sharp decrease near 700 hPa is caused by the northeasterly Harmattan winds in the LT, and the blocking Saharan anticyclone at higher altitudes which prevents vertical mixing over the source regions as shown in Fig. 23. The influence of these transport patterns on CO was first discussed by Jonquieres et al. (1998) who analyzed exploratory aircraft data from this region, and by Sauvage et al. (2005).

Figure 23 shows the transport patterns in February of 2005 and 2006. With the southward propagation of the ITCZ in this season, the Harmattan winds become stronger and penetrate to the Equator. The winds sweep up CO from the burning region and transport it over the Gulf of Guinea to the ITCZ where it is lofted by convection. By 200 hPa, the winds over the equatorial region change direction to south-westerly

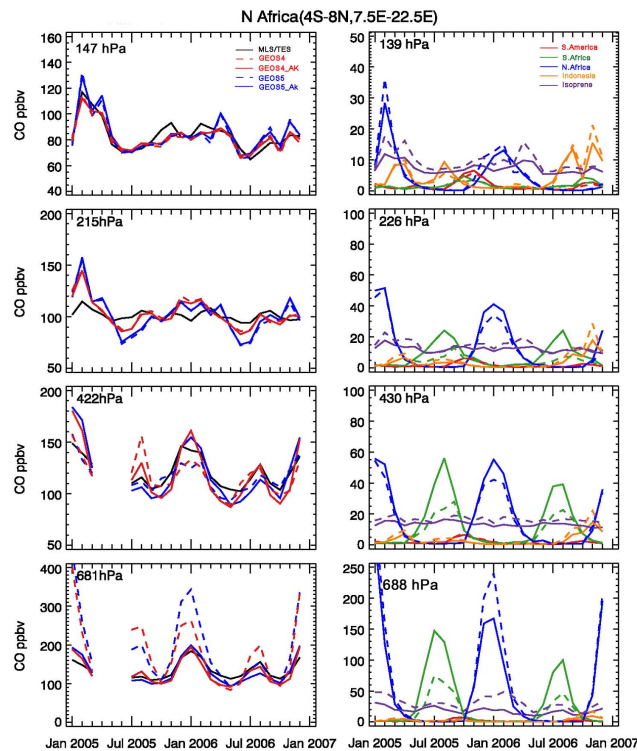


Fig. 21. Left: Time series of TES CO (681 and 422 hPa) and MLS CO (215 and 147 hPa), scaled as in Fig. 8) in (black) and model results for GEOS-4 (red) and GEOS-5 (blue) over northern Africa. Solid lines show the model results with the AKs applied, dashed lines show the model results without the AKs. Right: Time series of tagged CO tracers over northern Africa from individual sources: biomass burning in South America (red), southern Africa (green), northern Africa (blue) and Indonesia (orange), and the biogenic source from isoprene (purple).

and transport CO rich air back across West Africa above the burning region and beyond, towards the Middle East. This unique transport pattern over the northern Africa implies that CO accumulation in the UT above the fire region is mainly determined by the strength of Harmattan wind in the LT and the vertical mixing over the Gulf of Guinea. Thus, the CO overestimate seen in Figs. 5, 21 and 22 may result from the combined influence of too strong Harmattan winds in the LT and too strong vertical mixing over the Gulf of Guinea in the model. These deficiencies in transport are also responsible for the low CO in the boundary layer and the excess CO above, compared to the MOZAIC data.

As shown in Figs. 21 and 23, the primary CO maximum during boreal winter in 2005 is much larger than that in 2006 in the UT (particularly at 147 hPa) in both the model and observations. This is caused by higher emissions in January–February 2005 than in 2006 (Fig. 1), as well as by enhanced vertical mixing over the Gulf of Guinea in the UT in February 2005 (Figs. 23 and 24). As discussed above, the secondary CO maximum over the northern Africa in the LT and

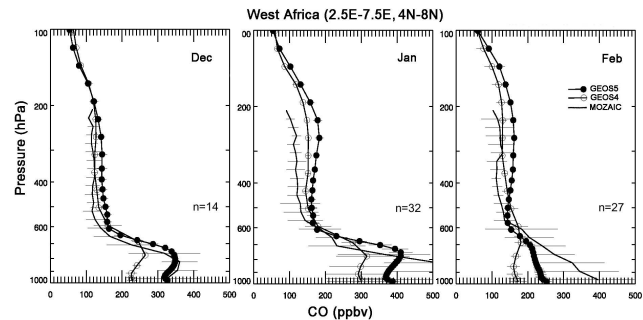


Fig. 22. Monthly mean CO profiles for December, January and February. MOZAIC aircraft profiles (solid line) are averages for 2002–2007 (primarily 2002–2004) over western Africa (Lagos, Abidjan, and Accra, $\sim 95\%$ from Lagos). n represents the numbers of observations at 520 hPa ($n=14$, 32, 27 for December, January and February). Model CO profiles are averages for 2005–2006 for the grid (2.5° E– 7.5° E, 4° N– 8° N) for GEOS-4 (open circles) and GEOS-5 (solid circles).

MT during boreal summer (Fig. 21) is caused by the collocation of the upward mass flux and high CO accumulated by transport of CO-laden air from the southern biomass burning by the strong southeasterly trade winds. By ~ 140 hPa, the maximum has shifted to October/November as a result of transport of CO from South America as well as southern Africa. Model CO is lower in the UT in GEOS-5 than in GEOS-4 in May to September because of less upward transport of CO from southern Africa. The underestimate of CO in June–July and the overestimate in December to February at 215 hPa causes the models to have a pronounced seasonal cycle, while there is none in the MLS data. The influence of CO from fires in southern Africa burning decreases with increasing altitude, and CO from Indonesian fires becomes an important source by 140 hPa (Fig. 21). Barret et al. (2008) suggests that westward transport of polluted air masses from Asia by the tropical easterly jet also contributes to CO above 150 hPa over northern Africa in summer. Increasing the CO sources in the southern continents causes an overestimate of CO over northern Africa in July–September in the MT, maximizing at 35–45 ppb in August, and in September–October at 215 hPa, in the GEOS-4 simulation (not shown); in the GEOS-5 run, the higher emissions lead to an improved simulation in the MT.

While the mechanisms transporting CO from the fires in northern Africa in boreal winter are well understood, the MLS data imply that the upward transport to the UT in the model is too strong in January and February, perhaps as a result of too strong Harmattan winds transporting CO to the ITCZ. The data show highest CO over the Gulf of Guinea and Nigeria in February in 2005, as do the GEOS-4 and GEOS-5 simulations, but the model peaks are about 30% too high; in 2006, the data shows a small peak in March, while in the GEOS-4 and -5 simulations it is in January.

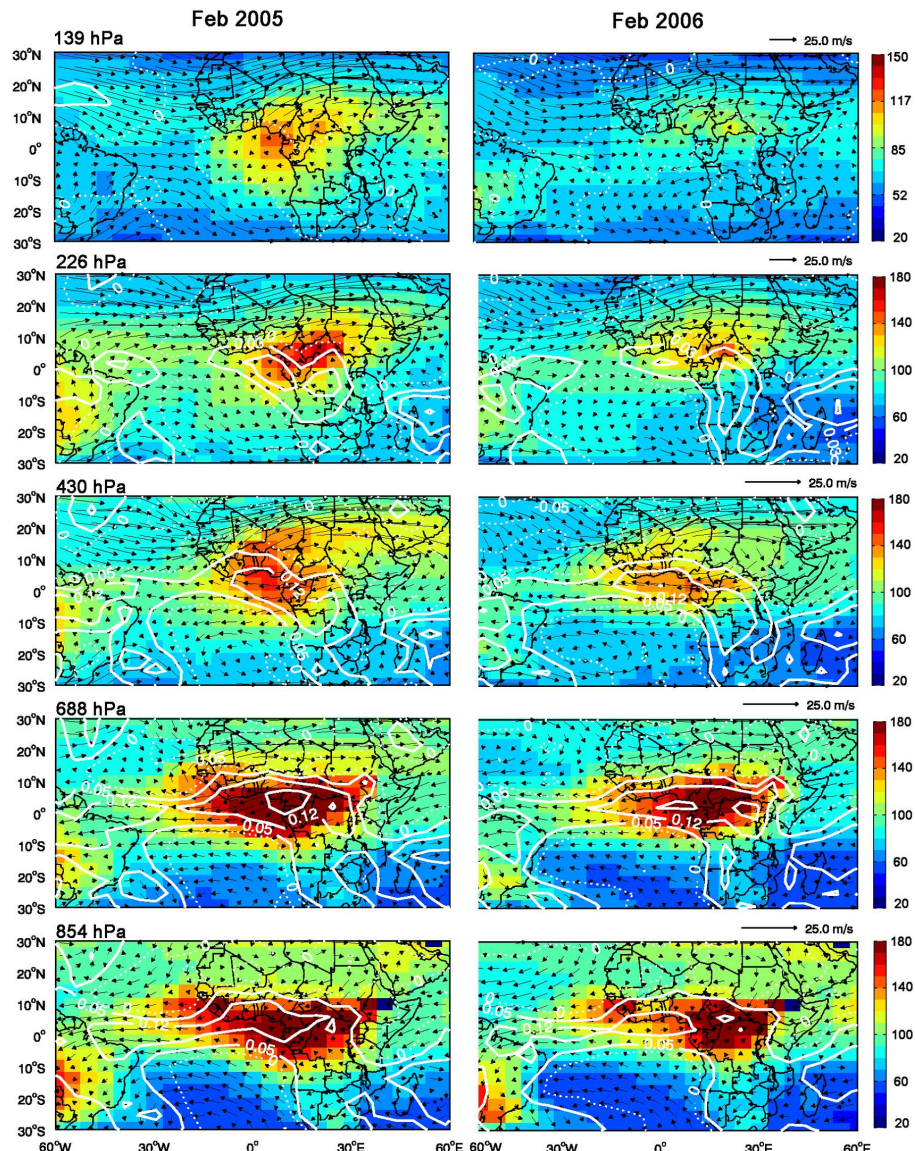


Fig. 23. CO mixing ratio overlaid with horizontal wind vectors in February 2005 and 2006 at 854, 688, 430, 226 and 139 hPa in for GEOS-4 simulations. The vertical air mass flux (Pa s^{-1}) is shown by contours: $(-0.05, 0, 0.05, 0.12, 0.2)$ for 854, 688, and 430 hPa, and $(-0.05, 0, 0.03, 0.06, 0.12)$ for 226 hPa. Positive values are upward fluxes (solid lines), negative values are downward fluxes (dashed).

5.4 Indonesia

The GEOS-4 and GEOS-5 simulations are very similar throughout the troposphere (Fig. 25). At the two lower levels, both simulations match the observed interannual variability and the timing of the CO maximum over Indonesia in 2006, although the peak is too narrow with a rapid decrease in CO after October. Nassar et al. (2009) also found that model CO in this region was too low in November in the LT. Their analysis of rainfall data implied that the GFED2 emissions decrease too rapidly in November at the end of the dry season.

In the UT, with the concern over the absolute accuracy of the MLS CO retrievals, we focus our analysis

on the difference between the CO maximum in October–November 2006 and the CO base-line during the previous 18 months. At 215 hPa, the models match the base-line, but the rapid increase in CO in October in both models is much larger than that in the observations, and we argue that this may result from too strong convection in the GEOS fields. Nassar et al. (2009) suggest that deep convection in GEOS-4 starts to increase in October over the Indonesia region about a month too early, based on their examination of data for outgoing long-wave radiation (OLR). At 147 hPa, CO from both models is in good agreement with the observed CO peak between September and November of 2006, but there is a systematic overestimate in the previous 18 months, so that the relative increase over the base-line is too small in

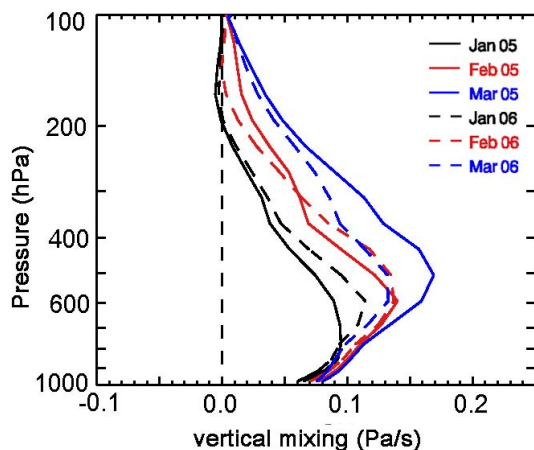


Fig. 24. Vertical profiles of total air mass flux (convection and advection) in GEOS-4 in the Gulf of Guinea from January to March in 2005 and 2006. Solid lines represent 2005 and dashed lines represent 2006.

October–November. Thus there is a larger decrease in model CO in October 2006 between 215 and 147 hPa than in the MLS observations. This implies that there is insufficient vertical mixing above 200 hPa in the models, but this result is contingent on the relative accuracy of the (scaled) MLS retrievals at 215 and 147 hPa.

6 Discussion and conclusions

In this study we used the GEOS-Chem model to interpret MLS and TES observations of the spatial and temporal variations of CO in the tropical troposphere for 2005 and 2006. Comparisons of the satellite observations and GEOS-Chem simulations, as well as analysis of the model meteorology and of tagged CO simulations, provide a detailed understanding of the interplay of convection and large scale ascent, as well as long-range transport, on CO emissions and thus on the model CO distribution. Our analysis also reveals flaws in aspects of tropical transport in the GEOS-4 and GEOS-5 meteorological fields, and in the isoprene emissions in the model, as well as successes.

The GEOS-Chem simulations capture many features of the morphology and seasonal variation of CO in the LT, although the models underestimate CO in the biomass burning season in eastern Amazonia and southern Africa, and in outflow to the Atlantic and Indian Oceans from these regions; conversely the models overestimate CO over western South America, south of 10° S, and over the equatorial eastern Pacific in August and September. In the UT, the seasonal maximum in model CO with GEOS-4 over South America occurs \sim 1 month later than the MLS maximum in 2005 and 2006, and with GEOS-5 it occurs \sim 1–2 months late in 2005 and \sim 3 months late in 2006. Our analysis shows that these

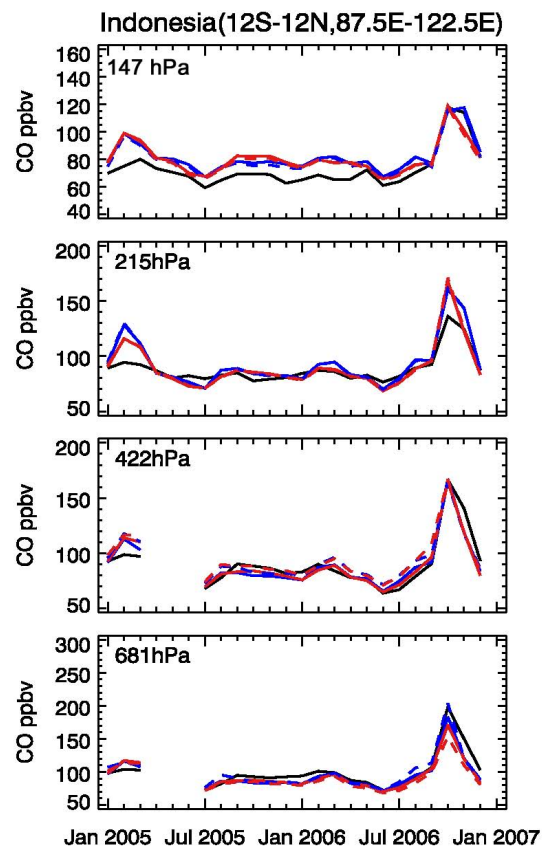


Fig. 25. Time series of TES CO (681 and 422 hPa) and MLS CO (215 and 147 hPa), scaled as in Fig. 8 (black) and model results for GEOS-4 (red) and GEOS-5 (blue) over Indonesia. Solid lines show the model results with the AKs applied, dashed lines show the model results without the AKs.

deficiencies are caused by two major factors: deep convection decays at too low an altitude in the UT, and the source of CO from isoprene in the model is too large in the wet season. The greater lag in GEOS-5 is in part because convection decays at a lower altitude, and in part because convection moves southward later than in GEOS-4. The CO peak from biomass burning at 147 hPa persists longer than the observed MLS peak, resulting from the dominant influence of slow large scale ascent in transporting this highly seasonal source in the tropical tropopause layer (TTL).

Our evaluation of the CO simulations implies that isoprene emissions from South America in MEGAN v2.1 as driven by the GEOS meteorological fields are too high for much of the year. The TES data shows a localized overestimate in model CO over western South America that is present from August to April, somewhat to the south of the geographic peak in isoprene emissions (Figs. 3 and 4). The overestimate is smallest, or missing, in May–July (not shown), when the isoprene emissions from South America in the model are smallest. Barkley et al. (2008) concluded from an analysis of satellite data for formaldehyde (HCHO), a degradation

product of isoprene oxidation, that isoprene emissions are very low in May–July. The MLS data also provide convincing evidence that the isoprene emissions in the model are too high, as they are responsible for the local maximum in CO at 215 hPa over South America from November to March that is present in the model simulations but not in the observations (Figs. 5 and 6). The isoprene source of CO also causes the lag of the CO seasonal maximum in the model UT compared to that in the MLS data as shown by the tagged CO results (Fig. 8). We note that an earlier MEGAN inventory (v2) also appeared to give too high emissions in Amazonia when implemented in GEOS-4, based on comparisons with aircraft and tower measurements of isoprene in that region (Barkley et al., 2008).

Increasing the CO emissions over South America and southern Africa following the results of the inverse analysis of Kopacz et al. (2010) was no panacea; while model CO matched the TES data in eastern Brazil, it was much too high in western South America and in the eastern Pacific. The discrepancy in the timing of the seasonal maximum between model and observations over South America remains at 147 hPa in both years. The inversion results of Kopacz et al. (2010) were dominated by AIRS data, and their comparison of the model results with a posteriori emissions to MO-PITT data also showed substantial overestimates in western South America and the eastern Pacific. Their inversion using MO-PITT data only showed similar problems but of a smaller magnitude.

Both the TES and MLS data revealed problems with excessive transport of CO to the eastern equatorial Pacific and lofting in the ITCZ in August and September, particularly in GEOS-4. These are the months with maximum fire emissions in South America and strong tropical south-easterlies in the lower troposphere in South America. Weaker easterly winds and weaker convection in the ITCZ in GEOS-5 result in a better simulation compared to GEOS-4 in this region, but for both models the results are worse when the surface emissions are increased in the sensitivity run. It is unclear if the high bias in CO in the eastern Pacific is caused primarily by overly strong easterlies, overly strong lofting of air in the ITCZ, or a combination.

The models were more successful in matching the phase of the observed CO variation throughout the troposphere over southern Africa. Isoprene does not contribute significantly to the seasonality of CO in the UT in this region. Its emissions are much smaller than those over South America, and vary less with season. The sensitivity run with increased emissions led to improved agreement with the magnitude of observed CO in the biomass burning season in the lower and middle troposphere, but caused an overestimate at 215 hPa in the GEOS-4 simulation. The difficulty in matching CO in the LT and UT implies there may be overly vigorous vertical transport early in the wet season. Comparison of the profiles of air mass fluxes indicate that convection detrains at a lower altitude in GEOS-5 than in GEOS-4. Vertical transport

over southern Africa in GEOS-5 at the end of the dry season may be more realistic than that in GEOS-4, as the sensitivity run with increased emissions shows better agreement with observed CO throughout the troposphere.

Over northern Africa, both models match the phase and magnitude of the CO variation rather well except at 215 hPa, where MLS does not show a seasonal cycle, while there is a winter maximum and a summer minimum in the models. Our analysis implies that the CO maximum in the UT above the fire region is mainly determined by the strength of low-level north-easterly Harmattan winds in the LT, vertical mixing over the Gulf of Guinea in the ITCZ, and transport back over north Africa in south-easterly flow in the MT and UT. The MLS data show that the models transport CO too vigorously to 215 hPa in January and February, either because the Harmattan winds are too strong, or in addition because the convection is too strong; the MOZAIC data support this argument. The secondary maximum in the MT during boreal summer is caused by the collocation of the ITCZ and high CO accumulated by transport from fires in southern Africa by strong southeasterly trade winds. The sensitivity run with increased emissions from southern Africa degrades the simulation over northern Africa in the MT, at least in GEOS-4. We chose not to adjust the emissions over northern Africa based on the results of Kopacz et al. (2010) (an increase of 40%) as it would clearly have exacerbated the discrepancies in the simulation of MLS and TES CO.

Over Indonesia, our analysis of vertical mixing in late 2006 using the MLS data substantiates the conclusions of Nassar et al. (2009) who relied on TES data only, and analysis of OLR data. They inferred that convection was too strong in GEOS-4 in October 2006, when the MLS data shows an overestimate in CO with both GEOS-4 and GEOS-5. Using the MLS data at both 147 and 215 hPa, we infer that there is insufficient vertical mixing above 200 hPa in the model in October and November 2006.

The GFED3 biomass burning inventory has recently been released (van der Werf et al., 2010). It uses a new data set for area burned (Giglio et al., 2010) as well as many improvements in the estimates for fuel consumption. The GFED3 CO emissions for South America are ~15% smaller than those from GFED2 in 2005 and similar in 2006; for Southern Africa, they are similar to GFED2 in 2005, and ~15% higher in 2006; and for northern Africa, they are ~15% lower than those in GFED2 in both years. The similarities between the GFED3 and GFED2 CO emissions in the tropics imply that the use of GFED3 emissions would not change the conclusions of our study. Clearly, difficulties remain in reconciling bottom-up and top-down estimates of CO emissions in the tropics even with these improved estimates of biomass burning emissions.

Our results have implications for the inverse methodology that has been widely used for constraining regional sources of CO (e.g. Arellano et al., 2004; Petron et al., 2004; Muller and Stavrakou, 2005; Arellano and Hess, 2006; Chevallier

et al., 2009; Jones et al., 2009), given that this approach does not account for biases in model transport. Kopacz et al. (2010) found that the constraints on tropical CO sources were not self-consistent when they used MOPITT, AIRS, and SCIAMACHY data separately, possibly due to the influence of different vertical sensitivities and retrieval approaches. Arellano and Hess (2006) examined the transport error in CO inversions by using two models and three sets of meteorological input (including GEOS-3). Within the tropics, the largest inconsistencies among the resulting source estimates were for South America and Indonesia, followed by southern Africa, and these are regions where we have identified some deficiencies with transport in the GEOS-4 and GEOS-5 fields. Indeed, Arellano and Hess noted significant differences in vertical transport in the three meteorological fields in their study. Our results suggest that caution is needed when using inverse methodology to estimate the uncertainties of different sources, especially in regions of where errors may be dominated by factors other than emissions, such as biases in transport.

Acknowledgements. This work was funded by NASA grants to Harvard University, NNX07AB17G, NNG06GB93G, and NNX09AJ41G. Work at the Jet Propulsion Laboratory, California Institute of Technology, was performed under contract with NASA. We thank Michael Barkley for his work on the implementation of MEGAN v2.1 in the GEOS-Chem model, and we thank M. Kopacz for providing emissions scaling factors. J. Liu would like to thank H. Liu, J. Jiang, L. Zhang, J. Fisher, and J. Mao for helpful discussions. The authors acknowledge the strong support of the European Commission, Airbus, and the Airlines (Lufthansa, Austrian, Air France) who carry free of charge the MOZAIC equipment and perform the maintenance since 1994. MOZAIC is presently funded by INSU-CNRS (France), Meteo-France, and Forschungszentrum (FZJ, Jülich, Germany). The MOZAIC database is supported by ETHER (CNES and INSU-CNRS).

Edited by: C. Gerbig

References

- Arellano, A. F. and Hess, P. G.: Sensitivity of top-down estimates of CO sources to GCTM transport, *Geophys. Res. Lett.*, 33, L21807, doi:10.1029/2006gl027371, 2006.
- Arellano, A. F., Kasibhatla, P. S., Giglio, L., van der Werf, G. R., and Randerson, J. T.: Top-down estimates of global CO sources using MOPITT measurements, *Geophys. Res. Lett.*, 31, L01104, doi:10.1029/2003gl018609, 2004.
- Barkley, M. P., Palmer, P. I., Kuhn, U., Kesselmeier, J., Chance, K., Kurosu, T. P., Martin, R. V., Helmig, D., and Guenther, A.: Net ecosystem fluxes of isoprene over tropical South America inferred from Global Ozone Monitoring Experiment (GOME) observations of HCHO columns, *J. Geophys. Res.-Atmos.*, 113, D20304, doi:10.1029/2008jd009863, 2008.
- Barret, B., Ricaud, P., Mari, C., Attié, J.-L., Bouscerez, N., Josse, B., Le Flochmoën, E., Livesey, N. J., Massart, S., Peuch, V.-H., Piacentini, A., Sauvage, B., Thouret, V., and Cammas, J.-P.: Transport pathways of CO in the African upper troposphere during the monsoon season: a study based upon the assimilation of spaceborne observations, *Atmos. Chem. Phys.*, 8, 3231–3246, doi:10.5194/acp-8-3231-2008, 2008.
- Barret, B., Williams, J. E., Bouarar, I., Yang, X., Josse, B., Law, K., Pham, M., Le Flochmoën, E., Liousse, C., Peuch, V. H., Carver, G. D., Pyle, J. A., Sauvage, B., van Velthoven, P., Schlager, H., Mari, C., and Cammas, J.-P.: Impact of West African Monsoon convective transport and lightning NO_x production upon the upper tropospheric composition: a multi-model study, *Atmos. Chem. Phys.*, 10, 5719–5738, doi:10.5194/acp-10-5719-2010, 2010.
- Beer, R.: TES on the Aura mission: Scientific objectives, measurements, and analysis overview, *Ieee T. Geosci. Remote*, 44, 1102–1105, doi:10.1109/tgrs.2005.863716, 2006.
- Beer, R., Glavich, T. A., and Rider, D. M.: Tropospheric emission spectrometer for the Earth Observing System's Aura Satellite, *Appl. Optics*, 40, 2356–2367, 2001.
- Bloom, S., da Silva, A., Dee, D., Bosilovich, M., Chern, J.-D., Pawson, S., Schubert, S., Sienkiewicz, M., Stajner, I., Tan, W.-W., and Wu, M.-L.: Documentation and Validation of the Goddard Earth Observing System (GEOS) Data Assimilation System – Version 4, Technical Report Series on Global Modeling and Data Assimilation NASA Goddard Space Flight Cent., Md, 2005.
- Bowman, K. W., Rodgers, C. D., Kulawik, S. S., Worden, J., Sarkissian, E., Osterman, G., Steck, T., Lou, M., Eldering, A., Shephard, M., Worden, H., Lampel, M., Clough, S., Brown, P., Rinsland, C., Gunson, M., and Beer, R.: Tropospheric emission spectrometer: Retrieval method and error analysis, *Ieee T. Geosci. Remote*, 44, 1297–1307, doi:10.1109/tgrs.2006871234, 2006.
- Chevallier, F., Fortems, A., Bousquet, P., Pison, I., Szopa, S., Devaux, M., and Hauglustaine, D. A.: African CO emissions between years 2000 and 2006 as estimated from MOPITT observations, *Biogeosciences*, 6, 103–111, doi:10.5194/bg-6-103-2009, 2009.
- Crutzen, P.: A discussion of the chemistry of some minor constituents in the stratosphere and troposphere, *Pure Appl. Geophys.*, 106, 1385–1399, doi:10.1007/BF00881092, 1973.
- Daniel, J. S. and Solomon, S.: On the climate forcing of carbon monoxide, *J. Geophys. Res.-Atmos.*, 103, 13249–13260, 1998.
- Duncan, B. N., Logan, J. A., Bey, I., Megretskaya, I. A., Yantosca, R. M., Novelli, P. C., Jones, N. B., and Rinsland, C. P.: Global budget of CO, 1988–1997: Source estimates and validation with a global model, *J. Geophys. Res.-Atmos.*, 112, D22301, doi:10.1029/2007jd008459, 2007.
- Edwards, D. P., Emmons, L. K., Gille, J. C., Chu, A., Attie, J. L., Giglio, L., Wood, S. W., Haywood, J., Deeter, M. N., Massie, S. T., Ziskin, D. C., and Drummond, J. R.: Satellite-observed pollution from Southern Hemisphere biomass burning, *J. Geophys. Res.-Atmos.*, 111, D14312, doi:10.1029/2005jd006655, 2006.
- Filipiak, M. J., Harwood, R. S., Jiang, J. H., Li, Q. B., Livesey, N. J., Manney, G. L., Read, W. G., Schwartz, M. J., Waters, J. W., and Wu, D. L.: Carbon monoxide measured by the EOS Microwave Limb Sounder on Aura: First results, *Geophys. Res. Lett.*, 32, L14825, doi:10.1029/2005gl022765, 2005.
- Folkins, I. and Martin, R. V.: The vertical structure of tropical convection and its impact on the budgets of water vapor and ozone, *J. Atmos. Sci.*, 62, 1560–1573, 2005.

- Folkins, I., Loewenstein, M., Podolske, J., Oltmans, S. J., and Profitt, M.: A barrier to vertical mixing at 14 km in the tropics: Evidence from ozonesondes and aircraft measurements, *J. Geophys. Res.-Atmos.*, 104, 22095–22102, 1999.
- Folkins, I., Braun, C., Thompson, A. M., and Witte, J.: Tropical ozone as an indicator of deep convection, *J. Geophys. Res.-Atmos.*, 107, D134184, doi:10.1029/2001jd001178, 2002.
- Folkins, I., Bernath, P., Boone, C., Donner, L. J., Eldering, A., Lesins, G., Martin, R. V., Sinnhuber, B. M., and Walker, K.: Testing convective parameterizations with tropical measurements of HNO_3 , CO , H_2O , and O_3 : Implications for the water vapor budget, *J. Geophys. Res.-Atmos.*, 111, D23304, doi:10.1029/2006jd007325, 2006.
- Fu, R., Zhu, B., and Dickinson, R. E.: How do atmosphere and land surface influence seasonal changes of convection in the tropical amazon?, *J. Climate*, 12(5), 1306–1321, 1999.
- Fu, R., Dickinson, R. E., Chen, M. X., and Wang, H.: How do tropical sea surface temperatures influence the seasonal distribution of precipitation in the equatorial Amazon?, *J. Climate*, 14, 4003–4026, 2001.
- Fu, R., Hu, Y. L., Wright, J. S., Jiang, J. H., Dickinson, R. E., Chen, M. X., Filipiak, M., Read, W. G., Waters, J. W., and Wu, D. L.: Short circuit of water vapor and polluted air to the global stratosphere by convective transport over the Tibetan Plateau, *P. Natl. Acad. Sci. USA*, 103, 5664–5669, doi:10.1073/pnas.0601584103, 2006.
- Fueglistaler, S., Dessler, A. E., Dunkerton, T. J., Folkins, I., Fu, Q., and Mote, P. W.: Tropical tropopause layer, *Rev. Geophys.*, 47, RG1004, doi:10.1029/2008rg000267, 2009.
- Giglio, L., Descloitres, J., Justice, C. O., and Kaufman, Y. J.: An enhanced contextual fire detection algorithm for MODIS, *Remote Sens. Environ.*, 87, 273–282, doi:10.1016/s0034-4257(03)00184-6, 2003.
- Giglio, L., van der Werf, G. R., Randerson, J. T., Collatz, G. J., and Kasibhatla, P.: Global estimation of burned area using MODIS active fire observations, *Atmos. Chem. Phys.*, 6, 957–974, doi:10.5194/acp-6-957-2006, 2006.
- Giglio, L., Randerson, J. T., van der Werf, G. R., Kasibhatla, P. S., Collatz, G. J., Morton, D. C., and DeFries, R. S.: Assessing variability and long-term trends in burned area by merging multiple satellite fire products, *Biogeosciences*, 7, 1171–1186, doi:10.5194/bg-7-1171-2010, 2010.
- Guenther, A. and Wiedinmyer, C.: User's guide to the Model of Emissions of Gases and Aerosols from Nature (MEGAN), Version 2.01, National Center for Atmospheric Research (NCAR), Boulder, Colorado, 2007.
- Guenther, A., Hewitt, C. N., Erickson, D., Fall, R., Geron, C., Graedel, T., Harley, P., Klinger, L., Lerdau, M., McKay, W. A., Pierce, T., Scholes, B., Steinbrecher, R., Tallamraju, R., Taylor, J., and Zimmerman, P.: A global model of natural volatile organic compound emissions, *J. Geophys. Res.-Atmos.*, 100, 8873–8892, 1995.
- Guenther, A., Baugh, B., Brasseur, G., Greenberg, J., Harley, P., Klinger, L., Serca, D., and Vierling, L.: Isoprene emission estimates and uncertainties for the Central African EXPRESSO study domain, *J. Geophys. Res.-Atmos.*, 104, 30625–30639, 1999.
- Guenther, A., Karl, T., Harley, P., Wiedinmyer, C., Palmer, P. I., and Geron, C.: Estimates of global terrestrial isoprene emissions using MEGAN (Model of Emissions of Gases and Aerosols from Nature), *Atmos. Chem. Phys.*, 6, 3181–3210, doi:10.5194/acp-6-3181-2006, 2006.
- Hack, J. J.: Parameterization of moist convection in the National Center for Atmospheric Research community climate model (CCM2), *J. Geophys. Res.-Atmos.*, 99, 5551–5568, 1994.
- Ho, S. P., Edwards, D. P., Gille, J. C., Luo, M., Osterman, G. B., Kulawik, S. S., and Worden, H.: A global comparison of carbon monoxide profiles and column amounts from Tropospheric Emission Spectrometer (TES) and Measurements of Pollution in the Troposphere (MOPITT), *J. Geophys. Res.-Atmos.*, 114, D21307, doi:10.1029/2009jd012242, 2009.
- Ito, A. and Akimoto, H.: Seasonal and interannual variations in CO and BC emissions from open biomass burning in Southern Africa during 1998–2005, *Global Biogeochem. Cy.*, 21, GB2011, doi:10.1029/2006gb002848, 2007.
- Jiang, J. H., Livesey, N. J., Su, H., Neary, L., McConnell, J. C., and Richards, N. A. D.: Connecting surface emissions, convective uplifting, and long-range transport of carbon monoxide in the upper troposphere: New observations from the Aura Microwave Limb Sounder, *Geophys. Res. Lett.*, 34, L18812, doi:10.1029/2007gl030638, 2007.
- Jones, D. B. A., Bowman, K. W., Logan, J. A., Heald, C. L., Liu, J., Luo, M., Worden, J., and Drummond, J.: The zonal structure of tropical O_3 and CO as observed by the Tropospheric Emission Spectrometer in November 2004 - Part 1: Inverse modeling of CO emissions, *Atmos. Chem. Phys.*, 9, 3547–3562, doi:10.5194/acp-9-3547-2009, 2009.
- Jonquieres, I., Marenco, A., Maalej, A., and Rohrer, F.: Study of ozone formation and transatlantic transport from biomass burning emissions over West Africa during the airborne Tropospheric Ozone Campaigns TROPOZ I and TROPOZ II, *J. Geophys. Res.-Atmos.*, 103, 19059–19073, 1998.
- Kar, J., Bremer, H., Drummond, J. R., Rochon, Y. J., Jones, D. B. A., Nichitiu, F., Zou, J., Liu, J., Gille, J. C., Edwards, D. P., Deeter, M. N., Francis, G., Ziskin, D., and Warner, J.: Evidence of vertical transport of carbon monoxide from Measurements of Pollution in the Troposphere (MOPITT), *Geophys. Res. Lett.*, 31, L23105, doi:10.1029/2004gl021128, 2004.
- Karoly, D. J. and Vincent, D. G.: Meteorology of the Southern Hemisphere, American Meteorological Society, 1998.
- Kopacz, M., Jacob, D. J., Fisher, J. A., Logan, J. A., Zhang, L., Megretskaya, I. A., Yantosca, R. M., Singh, K., Henze, D. K., Burrows, J. P., Buchwitz, M., Khlystova, I., McMillan, W. W., Gille, J. C., Edwards, D. P., Eldering, A., Thouret, V., and Nedelec, P.: Global estimates of CO sources with high resolution by adjoint inversion of multiple satellite datasets (MOPITT, AIRS, SCIAMACHY, TES), *Atmos. Chem. Phys.*, 10, 855–876, doi:10.5194/acp-10-855-2010, 2010.
- Kulawik, S. S., Worden, J., Eldering, A., Bowman, K., Gunson, M., Osterman, G. B., Zhang, L., Clough, S. A., Shepherd, M. W., and Beer, R.: Implementation of cloud retrievals for Tropospheric Emission Spectrometer (TES) atmospheric retrievals: part 1. Description and characterization of errors on trace gas retrievals, *J. Geophys. Res.-Atmos.*, 111, D24204, doi:10.1029/2005jd006733, 2006.

- Kulawik, S. S., Bowman, K. W., Luo, M., Rodgers, C. D., and Jourdain, L.: Impact of nonlinearity on changing the a priori of trace gas profile estimates from the Tropospheric Emission Spectrometer (TES), *Atmos. Chem. Phys.*, 8, 3081–3092, doi:10.5194/acp-8-3081-2008, 2008.
- Lawrence, M. G. and Salzmann, M.: On interpreting studies of tracer transport by deep cumulus convection and its effects on atmospheric chemistry, *Atmos. Chem. Phys.*, 8, 6037–6050, doi:10.5194/acp-8-6037-2008, 2008.
- Lelieveld, J., Berresheim, H., Borrmann, S., Crutzen, P. J., Dentener, F. J., Fischer, H., Feichter, J., Flatau, P. J., Heland, J., Holzinger, R., Korrman, R., Lawrence, M. G., Levin, Z., Markowicz, K. M., Mihalopoulos, N., Minikin, A., Ramanathan, V., de Reus, M., Roelofs, G. J., Scheeren, H. A., Sciare, J., Schlager, H., Schultz, M., Siegmund, P., Steil, B., Stephanou, E. G., Stier, P., Traub, M., Warneke, C., Williams, J., and Ziereis, H.: Global air pollution crossroads over the Mediterranean, *Science*, 298(5594), 794–799, 2002.
- Levy, H.: Normal atmosphere: large radical and formaldehyde concentrations predicted, *Science*, 173, 141–143, 1971.
- Li, Q. B., Jiang, J. H., Wu, D. L., Read, W. G., Livesey, N. J., Waters, J. W., Zhang, Y. S., Wang, B., Filipiak, M. J., Davis, C. P., Turquety, S., Wu, S. L., Park, R. J., Yantosca, R. M., and Jacob, D. J.: Convective outflow of South Asian pollution: A global CTM simulation compared with EOS MLS observations, *Geophys. Res. Lett.*, 32, L14826, doi:10.1029/2005gl022762, 2005.
- Liu, C. T., Zipser, E., Garrett, T., Jiang, J. H., and Su, H.: How do the water vapor and carbon monoxide “tape recorders” start near the tropical tropopause?, *Geophys. Res. Lett.*, 34, L09804, doi:10.1029/2006gl029234, 2007.
- Livesey, N. J., Read, W. G., Lambert, A., Cofield, R. E., and Cuddy, D. T.: EOS MLS version 2.2 Level 2 data quality and description document, Jet Propul. Lab., Pasadena, Calif, 2007.
- Livesey, N. J., Filipiak, M. J., Froidevaux, L., Read, W. G., Lambert, A., Santee, M. L., Jiang, J. H., Pumphrey, H. C., Waters, J. W., Cofield, R. E., Cuddy, D. T., Daffer, W. H., Drouin, B. J., Fuller, R. A., Jarnot, R. F., Jiang, Y. B., Knosp, B. W., Li, Q. B., Perun, V. S., Schwartz, M. J., Snyder, W. V., Stek, P. C., Thurstans, R. P., Wagner, P. A., Avery, M., Browell, E. V., Cammas, J. P., Christensen, L. E., Diskin, G. S., Gao, R. S., Jost, H. J., Loewenstein, M., Lopez, J. D., Nedelec, P., Osterman, G. B., Sachse, G. W., and Webster, C. R.: Validation of Aura Microwave Limb Sounder O₃ and CO observations in the upper troposphere and lower stratosphere, *J. Geophys. Res.-Atmos.*, 113, D15S02, doi:10.1029/2007jd008805, 2008.
- Logan, J. A., Prather, M. J., Wofsy, S. C., and McElroy, M. B.: Tropospheric chemistry: A global perspective, *J. Geophys. Res.-Oceans*, 86, 7210–7254, 1981.
- Logan, J. A., Megretskaya, I., Nassar, R., Murray, L. T., Zhang, L., Bowman, K. W., Worden, H. M., and Luo, M.: Effects of the 2006 El Niño on tropospheric composition as revealed by data from the Tropospheric Emission Spectrometer (TES), *Geophys. Res. Lett.*, 35, L03816, doi:10.1029/2007gl031698, 2008.
- Lopez, J. P., Luo, M., Christensen, L. E., Loewenstein, M., Jost, H., Webster, C. R., and Osterman, G.: TES carbon monoxide validation during two AVE campaigns using the Argus and ALIAS instruments on NASA’s WB-57F, *J. Geophys. Res.-Atmos.*, 113, D16S47, doi:10.1029/2007jd008811, 2008.
- Luo, M., Rinsland, C., Fisher, B., Sachse, G., Diskin, G., Logan, J., Worden, H., Kulawik, S., Osterman, G., Eldering, A., Herman, R., and Shephard, M.: TES carbon monoxide validation with DACOM aircraft measurements during INTEX-B 2006, *J. Geophys. Res.-Atmos.*, 112, D24S48, doi:10.1029/2007jd008803, 2007a.
- Luo, M., Rinsland, C. P., Rodgers, C. D., Logan, J. A., Worden, H., Kulawik, S., Eldering, A., Goldman, A., Shephard, M. W., Gunson, M., and Lampel, M.: Comparison of carbon monoxide measurements by TES and MOPITT: Influence of a priori data and instrument characteristics on nadir atmospheric species retrievals, *J. Geophys. Res.-Atmos.*, 112, D09303, doi:10.1029/2006jd007663, 2007b.
- Manabe, S., Hahn, D. G., and Holloway, J. L.: The seasonal variation of the tropical circulation as simulated by a global model of the atmosphere, *J. Atmos. Sci.*, 31, 43–83, 1974.
- Marenci, A., Medale, J. C., and Prieur, S.: Study of tropospheric ozone in the tropical belt (Africa, America) from STRATOZ and TROPOZ campaigns, *Atmos. Environ. A-Gen.*, 24, 2823–2834, doi:10.1016/0960-1686(90)90169-N, 1990.
- Marengo, J. A., Nobre, C. A., Tomasella, J., Oyama, M. D., De Oliveira, G. S., De Oliveira, R., Camargo, H., Alves, L. M., and Brown, I. F.: The drought of Amazonia in 2005, *J. Climate*, 21(3), 495–516, doi:10.1175/2007jcli1600.1, 2008.
- Martin, R. V., Sauvage, B., Folkins, I., Sioris, C. E., Boone, C., Bernath, P., and Ziemke, J.: Space-based constraints on the production of nitric oxide by lightning, *J. Geophys. Res.-Atmos.*, 112, D09309, doi:10.1029/2006jd007831, 2007.
- Miyoshi, A., Hatakeyama, S., and Washida, N.: OH radical-initiated photooxidation of isoprene: An estimate of global CO production, *J. Geophys. Res.-Atmos.*, 99, 18779–18787, doi:10.1029/94JD01334, 1994.
- Moorthi, S. and Suarez, M. J.: Relaxed Arakawa-Schubert: A parameterization of moist convection for general circulation models, *Mon. Weather Rev.*, 120, 978–1002, 1992.
- Müller, J.-F. and Stavrakou, T.: Inversion of CO and NO_x emissions using the adjoint of the IMAGES model, *Atmos. Chem. Phys.*, 5, 1157–1186, doi:10.5194/acp-5-1157-2005, 2005.
- Murray, L. T., Jacob, D. J., Logan, J. A., and Hudman, R. C.: Spatiotemporally constraining the lightning flash rate parameterization to satellite observations in a chemical transport model and its impact on variability in the oxidative capacity of the troposphere, in preparation, 2010.
- Nassar, R., Logan, J. A., Worden, H. M., Megretskaya, I. A., Bowman, K. W., Osterman, G. B., Thompson, A. M., Tarasick, D. W., Austin, S., Claude, H., Dubey, M. K., Hocking, W. K., Johnson, B. J., Joseph, E., Merrill, J., Morris, G. A., Newchurch, M., Oltmans, S. J., Posny, F., Schmidlin, F. J., Vomel, H., Whiteman, D. N., and Witte, J. C.: Validation of Tropospheric Emission Spectrometer (TES) nadir ozone profiles using ozonesonde measurements, *J. Geophys. Res.-Atmos.*, 113, D15S17, doi:10.1029/2007jd008819, 2008.
- Nassar, R., Logan, J. A., Megretskaya, I. A., Murray, L. T., Zhang, L., and Jones, D. B. A.: Analysis of tropical tropospheric ozone, carbon monoxide, and water vapor during the 2006 El Niño using TES observations and the GEOS-Chem model, *J. Geophys. Res.-Atmos.*, 114, D17304, doi:10.1029/2009jd011760, 2009.

- Nedelec, P., Cammas, J.-P., Thouret, V., Athier, G., Cousin, J.-M., Legrand, C., Abonnel, C., Lecoeur, F., Cayez, G., and Marizy, C.: An improved infrared carbon monoxide analyser for routine measurements aboard commercial Airbus aircraft: technical validation and first scientific results of the MOZAIC III programme, *Atmos. Chem. Phys.*, 3, 1551–1564, doi:10.5194/acp-3-1551-2003, 2003.
- Novelli, P. C., Masarie, K. A., Lang, P. M., Hall, B. D., Myers, R. C., and Elkins, J. W.: Reanalysis of tropospheric CO trends: Effects of the 1997–1998 wildfires, *J. Geophys. Res.-Atmos.*, 108, D154464, doi:10.1029/2002jd003031, 2003.
- Osterman, G.: Earth Observing System (EOS) Tropospheric Emission Spectrometer (TES) Data Validation Report (Version F04_04 data), Jet Propulsion Laboratory, California Institute of Technology, Pasadena, CA, 2007.
- Ott, L. E., Bacmeister, J., Pawson, S., Pickering, K., Stenchikov, G., Suarez, M., Huntrieser, H., Loewenstein, M., Lopez, J., and Xueref-Remy, I.: Analysis of Convective Transport and Parameter Sensitivity in a Single Column Version of the Goddard Earth Observation System, Version 5, General Circulation Model, *J. Atmos. Sci.*, 66, 627–646, doi:10.1175/2008jas2694.1, 2009.
- Panarello, H. O. and Dapena, C.: Large scale meteorological phenomena, ENSO and ITCZ, define the Parana River isotope composition, *J. Hydrol.*, 365, 105–112, doi:10.1016/j.jhydrol.2008.11.026, 2009.
- Park, M., Randel, W. J., Gettelman, A., Massie, S. T., and Jiang, J. H.: Transport above the Asian summer monsoon anticyclone inferred from Aura Microwave Limb Sounder tracers, *J. Geophys. Res.-Atmos.*, 112, D16309, doi:10.1029/2006jd008294, 2007.
- Park, M., Randel, W. J., Emmons, L. K., Bernath, P. F., Walker, K. A., and Boone, C. D.: Chemical isolation in the Asian monsoon anticyclone observed in Atmospheric Chemistry Experiment (ACE-FTS) data, *Atmos. Chem. Phys.*, 8, 757–764, doi:10.5194/acp-8-757-2008, 2008.
- Park, M., Randel, W. J., Emmons, L. K., and Livesey, N. J.: Transport pathways of carbon monoxide in the Asian summer monsoon diagnosed from Model of Ozone and Related Tracers (MOZART), *J. Geophys. Res.-Atmos.*, 114, D08303, doi:10.1029/2008jd010621, 2009.
- Petron, G., Granier, C., Khattatov, B., Yudin, V., Lamarque, J. F., Emmons, L., Gille, J., and Edwards, D. P.: Monthly CO surface sources inventory based on the 2000–2001 MOPITT satellite data, *Geophys. Res. Lett.*, 31, L21107, doi:10.1029/2004gl020560, 2004.
- Prinn, R. G., Huang, J., Weiss, R. F., Cunnold, D. M., Fraser, P. J., Simmonds, P. G., McCulloch, A., Harth, C., Salameh, P., O'Doherty, S., Wang, R. H. J., Porter, L., and Miller, B. R.: Evidence for substantial variations of atmospheric hydroxyl radicals in the past two decades, *Science*, 292(5523), 1882–1888, 2001.
- Prinn, R. G., Huang, J., Weiss, R. F., Cunnold, D. M., Fraser, P. J., Simmonds, P. G., McCulloch, A., Harth, C., Reimann, S., Salameh, P., O'Doherty, S., Wang, R. H. J., Porter, L. W., Miller, B. R., and Krummel, P. B.: Evidence for variability of atmospheric hydroxyl radicals over the past quarter century, *Geophys. Res. Lett.*, 32, L07809, doi:10.1029/2004gl022228, 2005.
- Rienecker, M., Suarez, M., Todling, R., Bacmeister, J., Takacs, L., Liu, H., Gu, W., Sienkiewicz, M., Koster, R., Gelaro, R., Stajner, I., and Nielsen, E.: The GEOS-5 Data Assimilation System - Documentation of Versions 5.0.1, 5.1.0, and 5.2.0, Technical Report Series on Global Modeling and Data Assimilation, NASA/TM-2007-104606, 2007.
- Rinsland, C. P., Luo, M., Logan, J. A., Beer, R., Worden, H., Kulawik, S. S., Rider, D., Osterman, G., Gunson, M., Eldering, A., Goldman, A., Shephard, M., Clough, S. A., Rodgers, C., Lampel, M., and Chiou, L.: Nadir measurements of carbon monoxide distributions by the Tropospheric Emission Spectrometer instrument onboard the Aura Spacecraft: Overview of analysis approach and examples of initial results, *Geophys. Res. Lett.*, 33, L22806, doi:10.1029/2006gl027000, 2006.
- Rinsland, C. P., Luo, M., Shephard, M. W., Clerbaux, C., Boone, C. D., Bernath, P. F., Chiou, L., and Coheur, P. F.: Tropospheric emission spectrometer (TES) and atmospheric chemistry experiment (ACE) measurements of tropospheric chemistry in tropical southeast Asia during a moderate El Nino in 2006, *J Quant. Spectrosc. Ra.*, 109, 1931–1942, doi:10.1016/j.jqsrt.2007.12.020, 2008.
- Rodgers, C. D.: Inverse Methods for Atmospheric Sounding: Theory and Practice, World Scientific, Singapore, 2000.
- Sakulyanontvittaya, T., Duhl, T., Wiedinmyer, C., Helmig, D., Matsunaga, S., Potosnak, M., Milford, J., and Guenther, A.: Monoterpene and sesquiterpene emission estimates for the United States, *Environ. Sci. Technol.*, 42, 1623–1629, doi:10.1021/es702274e, 2008.
- Sauvage, B., Thouret, V., Cammas, J.-P., Gheusi, F., Athier, G., and Nédélec, P.: Tropospheric ozone over Equatorial Africa: regional aspects from the MOZAIC data, *Atmos. Chem. Phys.*, 5, 311–335, doi:10.5194/acp-5-311-2005, 2005.
- Sauvage, B., Gheusi, F., Thouret, V., Cammas, J.-P., Duron, J., Escobar, J., Mari, C., Mascart, P., and Pont, V.: Medium-range mid-tropospheric transport of ozone and precursors over Africa: two numerical case studies in dry and wet seasons, *Atmos. Chem. Phys.*, 7, 5357–5370, doi:10.5194/acp-7-5357-2007, 2007a.
- Sauvage, B., Martin, R. V., van Donkelaar, A., Liu, X., Chance, K., Jaeglé, L., Palmer, P. I., Wu, S., and Fu, T.-M.: Remote sensed and in situ constraints on processes affecting tropical tropospheric ozone, *Atmos. Chem. Phys.*, 7, 815–838, doi:10.5194/acp-7-815-2007, 2007b.
- Schoeberl, M. R., Duncan, B. N., Douglass, A. R., Waters, J., Livesey, N., Read, W., and Filipiak, M.: The carbon monoxide tape recorder, *Geophys. Res. Lett.*, 33, L12811, doi:10.1029/2006gl026178, 2006.
- Shabanov, N. V., Huang, D., Yang, W. Z., Tan, B., Knyazikhin, Y., Myneni, R. B., Ahl, D. E., Gower, S. T., Huete, A. R., Aragao, L., and Shimabukuro, Y. E.: Analysis and optimization of the MODIS leaf area index algorithm retrievals over broadleaf forests, *Ieee T. Geosci. Remote.*, 43, 1855–1865, doi:10.1109/tgrs.2005.852477, 2005.
- Shindell, D. T., Faluvegi, G., Stevenson, D. S., Krol, M. C., Emmons, L. K., Lamarque, J. F., Petron, G., Dentener, F. J., Ellingsen, K., Schultz, M. G., Wild, O., Amann, M., Atherton, C. S., Bergmann, D. J., Bey, I., Butler, T., Cofala, J., Collins, W. J., Derwent, R. G., Doherty, R. M., Drevet, J., Eskes, H. J., Fiore, A. M., Gauss, M., Hauglustaine, D. A., Horowitz, L. W., Isaksen, I. S. A., Lawrence, M. G., Montanaro, V., Muller, J. F., Pitari, G., Prather, M. J., Pyle, J. A., Rast, S., Rodriguez, J. M., Sanderson, M. G., Savage, N. H., Strahan, S. E., Sudo, K., Szopa, S., Unger, N., van Noije, T. P. C., and Zeng, G.: Multimodel simulations of carbon monoxide: Comparison with observations and

- projected near-future changes, *J. Geophys. Res.-Atmos.*, 111, D19306, doi:10.1029/2006jd007100, 2006.
- Solomon, S., Qin, D., Manning, M., Chen, Z., Marquis, M., Averyt, K. B., Tignor, M., and Miller, H. L.: Climate change 2007: the Physical Science Basis. Contribution of Working Group I to the Fourth Assessment Report of the Intergovernmental Panel on Climate Change, 18 pp., 2007.
- Staudt, A. C., Jacob, D. J., Logan, J. A., Bachiochi, D., Krishnamurti, T. N., and Sachse, G. W.: Continental sources, transoceanic transport, and interhemispheric exchange of carbon monoxide over the Pacific, *J. Geophys. Res.-Atmos.*, 106, 32571–32589, 2001.
- Thorncroft, C. D. and Blackburn, M.: Maintenance of the African easterly jet, *Q. J. Roy. Meteor. Soc.*, 125, 763–786, 1999.
- van der Werf, G. R., Randerson, J. T., Giglio, L., Collatz, G. J., Kasibhatla, P. S., and Arellano Jr., A. F.: Interannual variability in global biomass burning emissions from 1997 to 2004, *Atmos. Chem. Phys.*, 6, 3423–3441, doi:10.5194/acp-6-3423-2006, 2006.
- van der Werf, G. R., Randerson, J. T., Giglio, L., Collatz, G. J., Mu, M., Kasibhatla, P. S., Morton, D. C., DeFries, R. S., Jin, Y., and van Leeuwen, T. T.: Global fire emissions and the contribution of deforestation, savanna, forest, agricultural, and peat fires (1997–2009), *Atmos. Chem. Phys.*, 10, 11707–11735, doi:10.5194/acp-10-11707-2010, 2010.
- Waters, J. W., Froidevaux, L., Harwood, R. S., Jarnot, R. F., Pickett, H. M., Read, W. G., Siegel, P. H., Cofield, R. E., Filipiak, M. J., Flower, D. A., Holden, J. R., Lau, G. K. K., Livesey, N. J., Manney, G. L., Pumphrey, H. C., Santee, M. L., Wu, D. L., Cuddy, D. T., Lay, R. R., Loo, M. S., Perun, V. S., Schwartz, M. J., Stek, P. C., Thurstans, R. P., Boyles, M. A., Chandra, K. M., Chavez, M. C., Chen, G. S., Chudasama, B. V., Dodge, R., Fuller, R. A., Girard, M. A., Jiang, J. H., Jiang, Y. B., Knosp, B. W., LaBelle, R. C., Lam, J. C., Lee, K. A., Miller, D., Oswald, J. E., Patel, N. C., Pukala, D. M., Quintero, O., Scaff, D. M., Van Snyder, W., Tope, M. C., Wagner, P. A., and Walch, M. J.: The Earth Observing System Microwave Limb Sounder (EOS MLS) on the Aura satellite, *Ieee T. Geosci. Remote*, 44, 1075–1092, doi:10.1109/tgrs.2006.873771, 2006.
- Williams, J. E., Scheele, M. P., van Velthoven, P. F. J., Cammas, J.-P., Thouret, V., Galy-Lacaux, C., and Volz-Thomas, A.: The influence of biogenic emissions from Africa on tropical tropospheric ozone during 2006: a global modeling study, *Atmos. Chem. Phys.*, 9, 5729–5749, doi:10.5194/acp-9-5729-2009, 2009.
- Worden, H., Beer, R., Bowman, K. W., Fisher, B., Luo, M., Rider, D., Sarkissian, E., Tremblay, D., and Zong, J.: TES level 1 algorithms: Interferogram processing, geolocation, radiometric, and spectral calibration, *Ieee T. Geosci. Remote*, 44, 1288–1296, doi:10.1109/tgrs.2005.863717, 2006.
- Worden, H. M., Logan, J. A., Worden, J. R., Beer, R., Bowman, K., Clough, S. A., Eldering, A., Fisher, B. M., Gunson, M. R., Herman, R. L., Kulawik, S. S., Lampel, M. C., Luo, M., Megretskaya, I. A., Osterman, G. B., and Shephard, M. W.: Comparisons of Tropospheric Emission Spectrometer (TES) ozone profiles to ozonesondes: Methods and initial results, *J. Geophys. Res.-Atmos.*, 112, D03309, doi:10.1029/2006jd007258, 2007.
- Yevich, R. and Logan, J. A.: An assessment of biofuel use and burning of agricultural waste in the developing world, *Global Biogeochem. Cy.*, 17(4), 1095, doi:10.1029/2002gb001952, 2003.
- Zeng, N., Yoon, J. H., Marengo, J. A., Subramaniam, A., Nobre, C. A., Mariotti, A., and Neelin, J. D.: Causes and impacts of the 2005 Amazon drought, *Environ. Res. Lett.*, 3, 014002, doi:10.1088/1748-9326/3/1/014002, 2008
- Zhang, G. J. and McFarlane, N. A.: Sensitivity of climate simulations to the parameterization of cumulus convection in the Canadian Climate Centre general circulation model, *Atmos. Ocean*, 33, 407–446, 1995.
- Zhang, L., Jacob, D. J., Bowman, K. W., Logan, J. A., Turquety, S., Hudman, R. C., Li, Q. B., Beer, R., Worden, H. M., Worden, J. R., Rinsland, C. P., Kulawik, S. S., Lampel, M. C., Shephard, M. W., Fisher, B. M., Eldering, A., and Avery, M. A.: Ozone-CO correlations determined by the TES satellite instrument in continental outflow regions, *Geophys. Res. Lett.*, 33, L18804, doi:10.1029/2006gl026399, 2006.